Mémoire

Auteur : Gourin, Thomas
Promoteur(s) : Jehin, Emmanuel
Faculté : Faculté des Sciences
Diplôme : Master en sciences spatiales, à finalité approfondie
Année académique : 2020-2021
URI/URL : http://hdl.handle.net/2268.2/12782

Faculty of Sciences

Department of Astrophysics, Geophysics and Oceanography

The automated SSOS pipeline:
further development and results

Thomas Gourin

A thesis presented for the degree of Master in Space Sciences

Supervisor
Emmanuel Jehin

Reading committee
Olivier Absil
Denis Grodent
Fransisco Pozuelos

Academic year 2020-2021

Acknowledgements

I would like to thank Emmanuel Jehin for his support throughout the year. Working independently on the TRAPPIST data has been enriching and I am grateful to you for letting me work freely.

I would also like to thank Marin Ferrais for his insights on the `Photometry Pipeline`, and Guillaume Sicorello for answering my questions on his work even at random times.

Finally, I would also like to thank my family and friends for their support during my studies, and in particular during this peculiar year.

Do I have to mention COVID-19?

Abstract

In this master thesis, we continued to develop and fine-tune the `automated SSOS pipeline` that can be automatically ran on the TRAPPIST images to search for serendipitous moving targets (asteroids and comets). We present the improvements that were made to the pipeline and its new functions (differential photometry and extraction of variable stars). The asteroids recovery capabilities have been significantly improved, having an efficiency of 100% up to magnitude 19, compared to magnitude 17 prior to these enhancements, and a detailed report is produced for each night. We also present a few lightcurves that were obtained and that allowed us to compute rotation periods of some asteroids.

Table of contents

Introduction

When the Solar System was formed around 4.6 billion years ago, its initial matter content was shared across various classes of objects, having various sizes, shapes and dynamics. From a molecular cloud, a proto-planetary system formed and its main objects have drastically evolved since then. Only the small Solar System bodies, the asteroids and comets, have not evolved much since their formation. They are thus considered as the remnants of the early Solar System.

Studying them help us to better understand this formation process as small bodies are the building blocks of the larger objects like the planets. Such process is universal and an analysis of their composition gives us also clues to the chemical conditions under which the planets and in particular the Earth formed. Moreover, as life is expected to have emerged from asteroid and comet impacts, their compositions provide information on the first molecules that could have played a role in the emergence of life.

Small bodies studies can be performed via numerous techniques: ground based or space borne observations, spacecraft directly sent to them or from the recoveries of meteorites that can be directly studied in a laboratory. Such event is very common, tons of dust fall on our planet every day, but only a fraction of objects reach the ground and are found before being contaminated by the environment. The probability is low but large objects have hit the Earth in the past and will continue to hit it in the future. In such cases, the impact could have catastrophic consequences for life on our planet. This is a more direct application of the study of small bodies: the monitoring of objects that are crossing Earth's orbit and that could potentially hit it, in order to participate to the planetary defense by identifying and characterising the most dangerous ones.

Object discoveries are mostly made by facilities dedicated to this task. With very performing telescopes and specialised computer tools, the number of newly discovered objects has skyrocketed in recent years. However, all optical telescopes that are dedicated to other scientific goals can catch asteroids in their images. Thus, having a pipeline that automatically searches for moving objects could give a further value to the countless images that are taken each night across the globe.

Last year, Sicorello, in his master thesis, used a freely available pipeline for this purpose and adapted it to the TRAPPIST-South images of the University of Liège [1]. We continued in this work to develop and improve the `automated SSOS pipeline` and present our own contributions to this topic in the following pages.

Starting with Chapter 1, we cover the scientific knowledge of the Solar System and define the various classes of asteroids and their locations.

In Chapter 2, we present the technical details that are used in the rest of this manuscript.

Chapter 3 makes the link with the work of Sicorello. We share the state of the art

and what direct improvements were made to his work.

In Chapter 4, we present what was newly built on the foundations discussed in the preceding chapter.

Finally, all our results are summarised in Chapter 5.

Chapter 1

General knowledge on the Solar System

In this first chapter, we give an overview of the scientific knowledge of the Solar System content throughout History, and the role the small bodies, and mainly the asteroids, plays in it.

1.1 Brief history of the observation of the Solar System content

In order to better understand the current knowledge of the Solar System content and before describing it, we retrace its scientific history since the first astronomers.

We start our story a long time ago. The night sky has never been completely dark and countless dots are illuminating the celestial vault. These small light dots were part of the development of civilizations throughout History. In the first societies, they were linked to faith and religion but they also proved useful in calendars and orientation.

In Ancient Greece, it was well known that not all the light dots were fixed in the sky. Indeed, night after night, season after season and year after year, almost all stars kept the same position with respect to the others. All except five of them, the so-called wandering stars. In the first scientific models, Greek astronomers placed the stars on a perfectly spherical and immutable heavenly sphere rotating around the Earth. The fact that their observations were no longer matching their model left them with no choice than to update it. The most lasting model was the one of Claudius Ptolemy (c.100-c.170), presented in the *Almagest*, a treaty on the motion of the stars. In it, Ptolemy presents the Solar System with the Earth in its center, and consecutive celestial spheres that allow the motion of the other known objects: the Moon, Mercury, Venus, the Sun, Mars, Jupiter, Saturn and finally the fixed stars. The problem of the reverse motion of the wandering stars was solved by Ptolemy who made use of deferents and epicycles[1], but shifted the position of the Earth which was no longer at the center of the deferents. Moreover, the epicycles were now moving at a constant speed with respect to a new point, the equant, which is

[1] A deferent is a celestial sphere, and an epicycle is a second sphere whose center moves on the deferent and which supports the motion of the objects it holds.

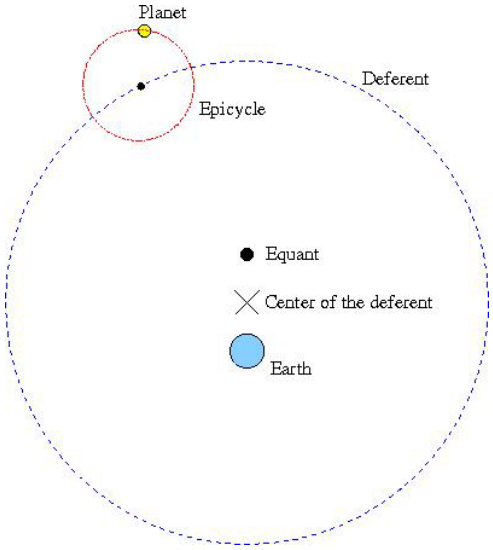

Figure 1.1: The Ptolemy model, making use of deferents and epicycles to justify the observed reverse motion of the visible planets (taken from the course *SPAT0036-1 Celestial mechanics and space trajectories*, G. Rauw, University of Liège, 2020-2021).

the symmetric point of the Earth with respect to the center of the deferents. This model is illustrated on Figure 1.1 for a more visual description and an easier understanding.

This geocentric view of the Solar System was the paradigm until Nicolaus Copernicus (1473-1543) reintroduced[2] the heliocentric model in 1543 in his work *De revolutionibus orbium coelestium*. However, his model was still far from the one we know today as Copernicus was still using the epicycles and deferents, and it was still not exactly matching the observations.

After him, Tycho Brahe (1546-1601) compiled a huge set of data of celestial positions having a newly reached precision. He looked for a mathematician who could use the data in order to confirm his geoheliocentric model, a model in which the Moon and the Sun are moving around the Earth, and all the other objects are moving around the Sun.

His assistant was the now famous Johannes Kepler (1571-1630). By studying the data obtained by Brahe for the motion of Mars, he concluded that it was moving around the Sun on an elliptical orbit. His results were published in *Astronomia Nova* in 1609 in which he presented his first two laws. His third law was published later, in 1919 in a second work titled *Harmonices mundi*.

Galileo Galilei (1564-1642) made his contribution with his observations in 1609 and 1610 of the moons of Jupiter, now known as the Galilean moons: Io, Europa, Ganymede, and Callisto. This discovery was a particular breakthrough in modern astronomy as these objects were the first that were orbiting neither the Sun nor the Earth.

In parallel, strange objects were observed in 1456, 1531, 1607 and 1682. Edmond Halley (1656-1742) concluded in 1705 that these observations were in fact of the same object. He also predicted that this object would come back in 1758, which was later confirmed with the observation of its return. These objects are now called comets because they are made of a coma in a direction opposite to the Sun, which is the reason they appear

[2]We purposely wrote that he *reintroduced* this model because he did not invent it, past astronomers had previously investigated this idea but the geocentric model was the paradigm until Copernicus' work.

strange to the observers of the past.

In 1800, a group of astronomers, the so-called "celestial police", were looking for the missing fifth planet. Indeed, two mathematicians previously noticed that the distances between the planets and the Sun were not random, and that they were following a rather elegant formula, the Titius-Bode law[3]:

$$d_n = 0.4 + 0.15 \cdot 2^n$$

with n the "number" of the planet ($-\infty$ for Mercury, 1 for Venus, 2 for the Earth and so on). Following this law, Jupiter would have to be the sixth planet for its distance to match the formula, and the Solar System would be missing a fifth planet at around 2.8 au from the Sun. As this formula had already proven its predictive aspect with the discovery of the eighth planet Uranus by William Herschel (1738-1822) in 1781, the celestial police was optimistic. And indeed, the law had again proven useful in 1801 with the discovery of Ceres by Giuseppe Piazzi (1746-1826). In the following years, other objects were observed in the vicinity of Ceres: Pallas in 1802, Junon in 1804 and Vesta in 1807 to name a few. As scientists were expecting to observe a planet, they kept the classification as-is until the 1850s when they had been redefined as asteroids. The term "asteroid belt" emerged in the same decade, and discoveries of new asteroids in this region of the Solar System kept to increase decades after decades.

Around the same time as this new definition, observations of Uranus showed that its position was not in agreement with predictions. Urbain Le Verrier (1811-1877) predicted the position of the perturbing body, and Johann G. Galle (1812-1910) discovered Neptune in 1846. However, the orbit of this newly found object was again perturbed, and the search for a yet again planet continued: astronomers were now looking for Planet X.

The discovery of the last "planet" of the Solar System is today attributed to Clyde W. Tombaugh (1906-1997) which discovered Pluto in 1930 with the help of a blink comparator[4]. Today, as we will define later, Pluto is no longer known as Planet X. Due to its very large distance from the Sun, astronomers could not manage to obtain information on its mass until the discovery of its satellite, Charon, in 1978. After this discovery, its mass was computed and found to be smaller than the mass of our Moon, meaning it was not the body perturbing the orbit of Neptune. Further discoveries of objects behind Pluto, with orbits as eccentric as its own, let some astronomers to consider this region as the Kuiper Belt, which is a region comparable to the asteroid belt.

But again, astronomers are not satisfied with the motion of the farthest objects in the Solar System. The original idea behind Planet X was to explain the observed motion of Uranus, but although Pluto is too small and the mass of Neptune was overestimated, some astronomers are today looking for Planet Nine. This time, the scientific reasoning behind the potential existence of this object is the strange grouping of trans Neptunian objects with similar orbits pointing in the same directions. Simulations show that we should also observe objects with orbits tilted almost to 90°, and we actually know five of them [2, 3]. Finally, Planet Nine could explain the orbital tilt of around 6° of the inner planets with

[3]Various expressions of this formula exist. Here, we present the one giving the distances from the Sun in astronomical units.

[4]A blink comparator is an apparatus with which we can rapidly switch between two photographs. This rapid switching allows to spot a change between the two images. In the case of the discovery of Pluto, Tombaugh was looking for the displacement of a light source.

respect to the Sun's equator. So astronomers are looking for a rocky Super-Earth with a mass ten times the one of our planet, which would be located approximately 20 times farther from the Sun than Neptune is. Other studies, based on an excess of micro-lensing events in the Optical Gravitational Lensing Experiment (OGLE) data, theorised that Planet Nine would not be a planet but a primordial black hole instead [4].

1.2 Formation of the Solar System

Now that we have presented a broad history of the discoveries of the bodies of the Solar System, let us present our current understanding of its formation until now.

The first true theory on the formation of the Solar System was the fruit of the work of Emanuel Swedenborg (1688-1772) and Immanuel Kant (1724-1804). The former developed the foundations of the nebular hypothesis and the latter finalised it. This hypothesis states that the Solar System started as a rotating gaseous cloud that collapsed through its own gravity and formed the Sun and the planets as we know them. At a similar time, Pierre-Simon Laplace (1749-1827) published his own scenario in 1796 in a work titled *Exposition du système du monde*. In it, Laplace presents the fact that the planets would have been formed by rings left by the Sun during its contraction.

The nebular hypothesis was the paradigm until the end of the 19th century. However, it was far from perfect. Indeed, it could not explain the angular momentum of the Sun which would have to be much higher compared to what is measured, and it could not explain precisely the formation of the terrestrial planets and Uranus and Neptune.

It was in 1969 that Viktor Safronov (1917-1999) proposed a more modern scenario: the core accretion model. It starts from the accepted nebular hypothesis, but the formation of the planets is more complex and accurate. As the cloud starts to collapse, its shape flatten due to the resultant force between gravitation and the Coriolis force. The proto-planetary system consists then of a proto-star surrounded by a disk of gas and dust. These dusts, with an original size of the order of a few micrometers, form larger objects through coagulation, the **planetesimals**, with size of the order of a few kilometers during a timespan of 1 to 2 million years. The planetesimals continue to grow through collisions and accretion until they reach a mass sufficient enough to attract and deflect nearby objects: this is the runaway growth. The heavier the object, the more it dominates the evolution of the system. We talk about **planetary embryos** once a planetesimal have reach the size of Mars, which takes roughly 2 to 3 million of years. The giant planets are first formed by collisions in around 5 to 10 millions of years and their high mass allow them to continue to accrete the surrounding gas. The terrestrial planets are formed after in around 10 to 100 millions of years.

Complementary theories have been built to supplement the core accretion model: the Grand Tack [5] and Nice models [6, 7, 8]. The former states that Jupiter was formed at around 3.5 au from the Sun and migrated inwards through a type II migration[5]. Jupiter was followed by Saturn and they entered a 3:2 resonance. As time passes, they slowly migrated outwards until the depletion of the disk. This scenario explains the small mass of Mars as its potential material was accreted by the two giants, and it can also explain

[5]A type II migration happens when a massive planet creates a hole in the disk when accreting material.

the origin of the water on Earth as the giants could bring icy material by deflecting objects from the outer Solar System. Finally, the Nice model states that the four forming giants planets, initially ordered Jupiter, Saturn, Neptune and Uranus, were orbiting between 5.5 and 17 au with other planetesimals beyond. In this theory, Jupiter and Saturn went into 1:2 resonance while Neptune went behind Uranus which destabilized the planetesimals disk. The four giants, now ordered inwards as of today: Neptune, Uranus, Saturn and Jupiter; could then capture progressively the incoming planetesimals which had for result to send them in the inner Solar System. The high mass of their final partner, Jupiter, send them to very wide and eccentric orbits. The giants reached their final orbits through the exchange of angular momentum: only the orbit of Jupiter was shortened whereas the other were lengthen.

1.3 The Solar System content

Now that we understand better the formation of the Solar System, we can properly define all of its content. As we have seen in the first section, some definitions were debatable: Ceres has rapidly lost its status of planet to be newly defined as an asteroid, and Pluto lost its status of planet in 2006, more than 70 years after its discovery.

First, the main object of the Solar System is obviously the Sun itself, which is a **star**, a giant ball of hot plasma.

As we have discussed in the previous section, the Solar System is made of **planets**, some of which are terrestrial like the Earth, while others are gas giants like Jupiter. The definition of a planet has been corrected in 2006 by the International Astronomical Union (IAU)[6] because of Pluto. Indeed, although Ceres and other similar objects had already been demoted from the status of planet, Pluto was considered as the ninth planet of the Solar System since its discovery in 1930. As we have previously discussed in the previous sections, the discovery of Charon and of other objects in this distant region made some astronomers no longer consider Pluto as a planet, and new definitions were precisely made by the IAU and are recalled hereafter.

A classical planet:

1. is in orbit around the Sun,
2. has sufficient mass for its self-gravity to overcome rigid body forces so that it assumes a hydrostatic equilibrium (nearly round) shape,
3. has cleared the neighbourhood around its orbit.

Pluto was then redefined as a **dwarf-planet** by the IAU. A dwarf-planet only checks the first two characteristics of a planet, meaning it has not cleared its neighbourhood.

[6] `https://www.iau.org/news/pressreleases/detail/iau0602/`

Precisely, a dwarf-planet:

1. is in orbit around the Sun,
2. has sufficient mass for its self-gravity to overcome rigid body, forces so that it assumes a hydrostatic equilibrium (nearly round) shape,
3. has not cleared the neighbourhood around its orbit,
4. is not a satellite.

The main object of the asteroid belt, Ceres, is therefore no longer considered as an asteroid but as a dwarf-planet, because its mass is high enough for it to be spherical. This is not the case for the other big objects of the asteroid belt, like Pallas, Vesta and Junon, which are sill considered as asteroids.

Speaking of which, **asteroids** fall in the category of the **small Solar System bodies**. According to the IAU, their definition is plain and simple:

All other objects, except satellites, orbiting the Sun shall be referred to collectively as "Small Solar System Bodies".

Therefore, as the small bodies are neither planets, satellites nor dwarf-planets, they encompass a broad spectrum of objects, from the asteroids, the Kuiper Belt objects, passing through the comets etc...

1.4 The various classes of asteroids

As our work was on the search of small Solar System bodies, and asteroids in particular, we dedicate this section to present their various classes and where they can be found in the Solar System.

1.4.1 The Main Asteroid Belt

Most asteroids are located in the **Main Asteroid Belt (MAB)**, which spans between 2 and 3.5 au from the Sun. As of June 1st, 2021, the MAB contains 1 028 696 main belt asteroids[7] (MABs) that are the remnants of a planet that was never formed due to the gravitational influence of Jupiter. For this reason, the bodies in this region have similar eccentricities and inclination: respectively 0.17 and 8.2° on average, in addition to similar semi-major axis. Furthermore, by plotting these three parameters in a 3D diagram, we notice that we have groups of asteroids. It was Kiyotsugu Hirayama (1874-1943) who discovered this feature in 1918 and identified the Koronis, Eos and Themis families [9]. These families have their origins in the destruction of at least one planetesimal per family. For example, a collision between two planetesimals broke them into smaller pieces which all followed more or less the same trajectory, and the current dispersion of the family members can give clues to the parent body and the collision itself (like the age and the velocity of the impact).

[7] https://minorplanetcenter.net/mpc/summary, visited on July 25th, 2021

Another peculiar feature of the Main Belt is the presence of gaps inside of it. We have four main gaps at 2.50, 2.82, 2.96 and 3.28 au, which do not correspond to forbidden heliocentric distances but rather to forbidden orbital periods [10]. Indeed, as the asteroids are under the gravitational influence of Jupiter, the corresponding resonances of 3:1, 5:2, 7:3 and 2:1 have ejected the asteroids in these regions outside of the Main Belt, some of which went into the inner Solar System to produce the Near Earth Asteroids population.

1.4.2 The Near-Earth Asteroids

The **Near-EArth Asteroids (NEAs)** have orbits with a perihelion $q < 1.3$ au. They can be classified into four classes:

1. the **Atiras** whose orbits are inside the one of the Earth. They have a semi-major axis $a < 1$ and an apelion distance $Q < 0.983$ au;

2. the **Atens** which cross the orbit of the Earth but with a semi-major axis $a < 1$ and an apelion distance $Q > 0.983$;

3. the **Apollos** also cross the orbit of the Earth but with a semi-major axis $a > 1$ and a perihelion distance $q < 1.017$;

4. the **Amors** whose orbits are outside the one of the Earth. They have a semi-major axis $a > 1$ and a perihelion distance $1.017 < q < 1.3$ au.

These classes are respectively named after their prototypes: (163693) Atira, (2026) Aten, (1862) Apollo and (1221) Amor.

Because some NEAs cross the orbit of the Earth, it is possible to have an encounter. Scientists estimate that each day, between 5 to 300 tonnes of material fall on Earth [11]. The grand public never hears of it in the news because this material is mainly dust and very small meteorites. However, bigger objects could hit the Earth and wreck havoc on the surface. Fortunately, the bigger the asteroid, the lower the frequency of impact [12, 13]. Astronomers are looking at **Potential Hazardous Asteroids (PHAs)**, which are NEAs whose Minimum Orbit Intersection Distance (MOID) with the Earth is less than 0.05 au and that have an absolute magnitude less or equal to 22, which means that they are both very close and sufficiently big (we use the rule of thumb that a bigger asteroid reflects more light and is therefore brighter[8]).

In terms of numbers, as of June 1st, 2021, we count: 26 420 NEAs which are subdivided into 48 Atiras, 2043 Atens, 13 388 Apollos and 10 939 Amors. A total of 941 of these asteroids are more than one kilometer in size, and 2263 are PHAs[9].

1.4.3 The trojans

The **trojans** are asteroids that have been captured by a planet. Historically, this class of objects was defined when astronomers observed asteroids at the Lagrange points[10] L_4

[8] In reality, we also have to consider the composition of the asteroid in order to have an accurate value of its albedo.

[9] https://minorplanetcenter.net/mpc/summary, visited on July 25th, 2021

[10] The Lagrange points are a set of five balanced solutions to the restricted three body problem.

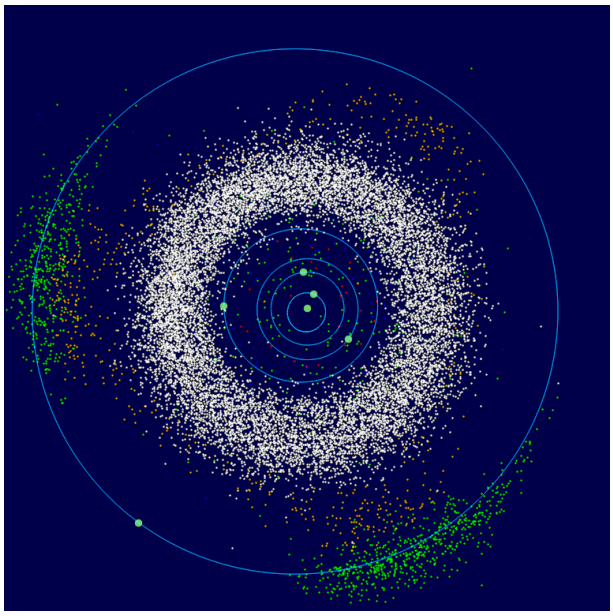

Figure 1.2: Representation of the asteroids of the inner Solar System up to the orbit of Jupiter. From the center we have the Sun with the four terrestrial planets orbiting around it and the NEAs in red. The MAB is the white doughnut. The Hilda family is in orange and the Jovian trojans are in green (taken from `https://commons.wikimedia.org/wiki/File:InnerSolarSystem.png`).

and L_5 of Jupiter. In the special case of Jupiter, the trojans that are in advance on the orbit are named after Greek figures whereas the trojans that are behind on the orbits are named after Trojan figures, the only two exceptions being the Greek (624) Hector and the Trojan (617) Patroclus [14]. As of June 1st, 2021, we count 10 520 Jupiter trojans[11].

Today, the concept of trojans can be generalised to other planets as they have been detected at other Lagrange points:

1. one for the Earth: 2010 TK_7 was confirmed in 2011 and is located at its L_4 point [15];
2. four for Mars, with potentially three more yet to be accepted by the MPC [16];
3. two for Uranus [17];
4. 28 for Neptune[12].

Moreover, such asteroids are bound to their planet, while others can librate at the Lagrange point only for a time. If the flux of incoming bodies is equivalent to the flux of leaving ones, we can have a population of transient trojans that is in steady state. This has been shown to happen in the MAB, with 129 MBAs entering in resonance with Ceres and 94 with (4) Vesta, with a lifetime of resonance of a few 10^5 yrs [18].

[11] https://minorplanetcenter.net/mpc/summary, visited on July 25th, 2021
[12] `https://minorplanetcenter.net//iau/lists/NeptuneTrojans.html`

1.4.4 The Hilda family

The **Hilda family**, named after the asteroid (153) Hilda, is located between the MBA and the orbit of Jupiter. They all are in a 3:2 resonance with the gas giant. Their elliptical orbit make them pass at three checkpoints during their three orbits: the first is located at the opposite of Jupiter at its L_3 point, the second is located at the L_4 point and the third is located at the L_5 point. As of June 1st, 2021, there are 4983 confirmed asteroids in this family[13], which form an instantaneous triangular shape between the three Lagrange points as it can be seen on Figure 1.2.

1.4.5 The Centaurs

The **Centaurs** orbit between Jupiter and Neptune ($q > 5.2$ au and $a < 30$ au). Due to their distance to the Sun, they are icy and their name comes from the mythological centaurs, half-man and half-horse creatures. Here, the centaurs are classified in-between the rocky asteroids and the icy comets.

Because their orbits are under the gravitational influence of the giant planets, they are unstable and the mean half-life of the population is of 2.7 million years before they can eventually be sent outside of the Solar System [19]. However, a study of the centaur (514107) 2015 BZ509 showed that it could be in a stable retrograde orbit since the formation of the Solar System, suggesting a potential interstellar origin [20]. A second paper published by the same authors draws the same conclusion for two other centaurs [21]. A more recent paper suggests that the populations of retrograde orbiting centaurs could be explained by NEAs that were ejected to the outer Solar System and deflected by Jupiter [22]. A second one directly challenges the interstellar origin of (514107) 2015 BZ509 and the other two centaurs, pointing to flaws in the argumentation [23]. The criticism is as follows: (1) backward simulations up to 4.5 Gyr are not a valid argument to explain the origin of a population due to dynamical instabilities (instead, simulations should be performed forward), (2) (514107) 2015 BZ509 being the sole survivor of a population of a million objects of size between 3 to 4 km, i.e. a population ten times larger than the equivalent population in the MAB, would be doubtful considering the expected density of interstellar planetesimals [24], (3) (514107) 2015 BZ509 could simply be a representative of a transient population in steady state, which could find its origin in the Oort Cloud or in the Halley-type comets. In summary, the only confirmed interstellar objects are the interstellar asteroid 1I/2017 U1 (Oumuamua) [25] (which was initially thought to be an interstellar comet [26]) and the confirmed interstellar comet C/2019 Q4 (Borisov) [27].

1.4.6 The Trans Neptunian Objects

The **Trans Neptunian Objects (TNOs)** are found behind the orbit of Neptune (a > 30 au) and can be classified into two subgroups: the **Kuiper belt objects (KBOs)** and the **Scattered disk objects (SDOs)**.

The Kuiper Belt spans from 30 to 50 au and is comparable to the Asteroid Belt, due to its circular shape and low inclination (although it is 20 times wider and between 20

[13] https://minorplanetcenter.net/mpc/summary, visited on July 25th, 2021

[14] `https://minorplanetcenter.net/mpc/summary`, visited on July 25th, 2021. We wrote "distant objects" as the MPC does not make the sub-classifications as of this date.

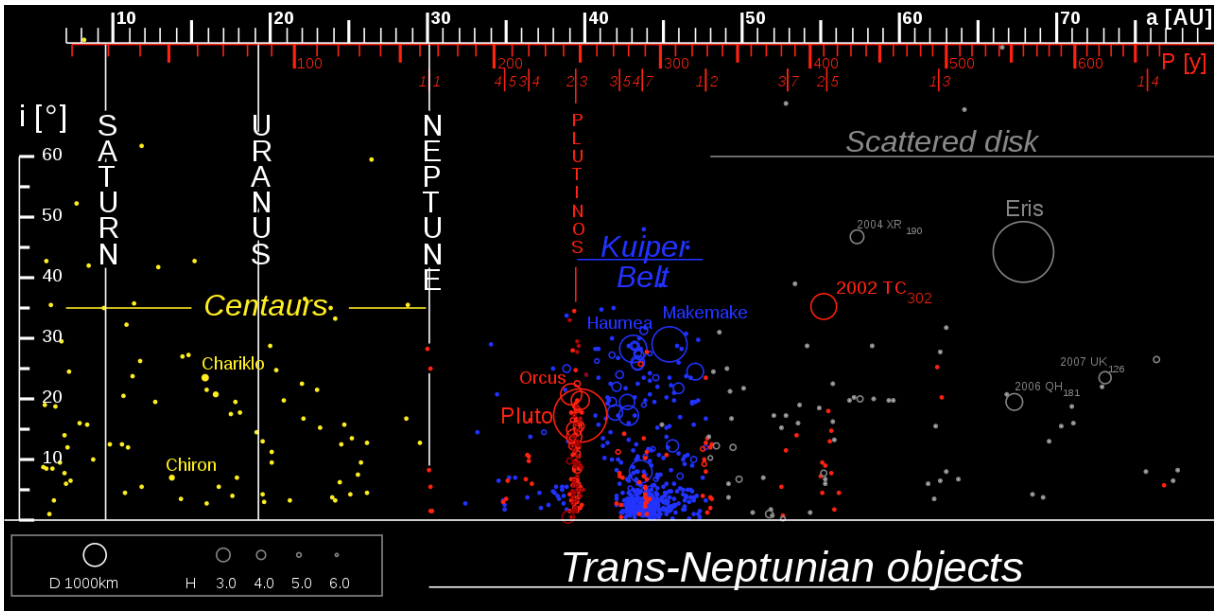

Figure 1.3: Representation of the different classes of asteroids of the outer Solar System as a function of their semi-major axis a (au) and inclination i (°). The Centaurs are in yellow, up to the orbit of Neptune at 30 au. The KBOs are in red (plutinos) and in blue (cubewanos). The SDOs are in grey. As of June 1st, 2021, we count 4052 distant objects[14](taken from `https://commons.wikimedia.org/wiki/File:TheTransneptunians_73AU.svg`).

to 200 times more massive). KBOs are classified with respect to their interactions with Neptune: they can be in resonance or not. If they are in 2:3 orbital resonance like Pluto, they are called **plutinos**. If they are in 1:1 resonance, they are trojans of Neptune and are call **twotinos**. If they are not in resonance, we talk about **cubewanos**.

The Scattered Disk is not comparable to the two belts due to the high eccentricities and inclinations of the objects it harbours. As it starts to span further than 50 au from the Sun, SDOs are not in resonance with nor crossing the orbits of any planet. Again, SDOs can be further divided according to their Tisserand invariant (T_P).

The Tisserand invariant of an asteroid with an orbit of semi-major axis a, eccentricity e and inclination i that is under the influence of a planet P with a semi-major axis a_P, is defined as:

$$T_P = \frac{a_P}{a} + 2\sqrt{\frac{a(1-e^2)}{a_P}}\cos i$$

Computing the Tissserand invariant for Neptune (N) allows to distinguish objects with $T_N < 3$ which are called **scattered-near** whereas objects with $T_N > 3$ are called **scattered-extended** [28].

1.5 The Oort Cloud

At much higher heliocentric distances, sufficiently far to cross the heliosphere and be outside of the Solar System, we can found the **Oort Cloud**, starting at best at around 2000 au from the Sun [29]. This is the reservoir of the **Long Period Comets (LPCs)**

[30]. Its existence is only theoretical as no direct observations were made, but its existence is suggested by the isotropic distribution of the inclinations of the LPCs. As comets were not part of our work (see Chapter 3), we end this chapter here.

Chapter 2

Theoretical and technical details

In this chapter, we give some reminders on orbital elements and astrometry. We present TRAPPIST-South, the telescope that was mainly used to produce the data that we analysed. Finally, we cover the photometry and lightcurve analysis of asteroids.

2.1 Orbital elements and astrometry

We start by recalling the orbital elements and explaining the principles of astrometry.

In classical mechanics, when characterising the state of a system, we need a set of six parameters. In celestial mechanics, in the case of the two-body problem, the lighter body follows a conic around the other according to Kepler's law. In that case, we can define a set of six parameters for any Keplerian motion: $(a, e, i, \Omega, \omega, \nu)$.

We have two parameters related to the shape of the orbit: the semi-major axis a and the eccentricity e. The inclination i characterises the angle between the orbit and a plane of reference. In the Solar System, the inclination is measured from the plane of the ecliptic, which is the plane where the orbit of the Earth lies (the inclination of the orbit of the Earth is thus equal to zero). The longitude of the ascending node Ω is the angle between a reference point and the ascending node, which is the point at which the moving body crosses the plane of reference upwards. The argument of pericenter ω defines the angle between the ascending node and the point of closest approach, the pericenter. Finally, the true anomaly ν corresponds to the position of the moving body along its orbit. A geometrical representation of these parameters can be found on the left panel of Figure 2.1. This set of parameter is particularly useful as five of them are related to the orbit itself and are constant, which leaves only the true anomaly to vary.

In the case of our work, we are mainly looking for asteroids. As we are observing from the Earth which orbits the Sun and as the asteroids themselves orbit it, the relative motion is quite complex. Fortunately, we can only consider the apparent position of the object with respect to a point of reference.

We define first the celestial plane, which corresponds to the plane of the equator. As the Earth axis is slightly tilted, this plane is different from the ecliptic plane. We define a set of two coordinates which are independent of the observer: the right ascension and declination (RA, DEC). The right ascension is the angle measured alongside the celestial plane from the point where the Sun crosses the celestial plane upwards (at the vernal

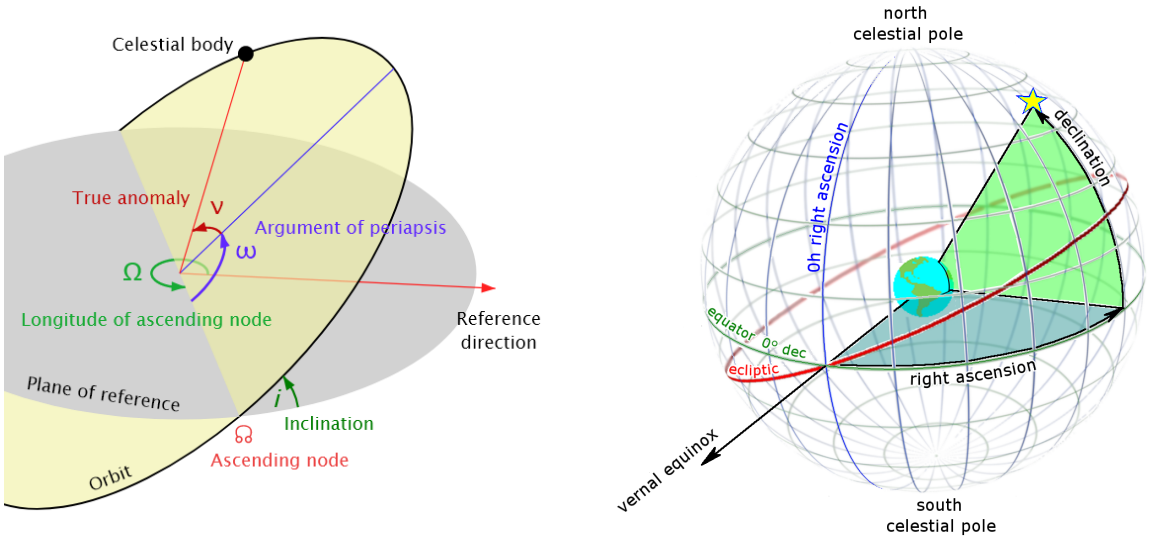

Figure 2.1: Left: 5 Keplerian elements describing the orbit, the semi-major axis a not being represented (taken from `https://commons.wikimedia.org/wiki/File:Orbit1.svg`). Right: geometrical definition of the right ascension and declination (taken from `https://commons.wikimedia.org/wiki/File:Ra_and_dec_on_celestial_sphere.png`).

equinox in March) to the position of the object on the celestial plane. The declination is the angle from this point to the object. A geometric example of this definition can be found on the right panel of Figure 2.1.

The right ascension is measured in hours-minutes-seconds (hms) whereas the declination, is measured in degrees-minutes-seconds (dms).

Astrometry is performed directly on site as the images are taken. Using a program like DC-3 Pinpoint[15] in the case of TRAPPIST, each pixel (x,y) can be linked to a position (RA,DEC) in the sky. When the observation is made, the stars that are present in the field can automatically be linked to catalogued coordinates in order to plate solve each image.

In the case of asteroid studies, knowing precisely the position of the objects is particularly important. Indeed, each measurement for each object can be sent to the MPC which uses the coordinates to constraint their orbits. Data files containing the orbital elements of all asteroids are available on the MPC webpages[16]. They are updated daily and are available for a range of minus to plus 15 days from the visit date. Knowing the future position of an object allows to do follow-up observations and knowing its orbital motion allows to perform numerical simulations in order to better understand its dynamics.

2.2 Instrumentation

In this work, we have been working mainly with the TRAPPIST-South telescope, which we are going to present and describe hereafter.

[15] `http://pinpoint.dc3.com/`
[16] `https://www.minorplanetcenter.net/data`

The TRAnsiting Planets and PlanetesImals Small Telescope (TRAPPIST)[17] is a project directed by the Origins in Cosmology and Astrophysics group (OrCA) of the Department of Astrophysics, Geophysics and Oceanography (AGO) of the STAR Institute of the University of Liège [31]. The TRAPPISTs are a pair of telescopes, TRAPPIST-South (TS) and TRAPPIST-North (TN), the former being located at the La Silla Observatory (Chile) and the latter at the Oukaïmeden Observatory (Morocco). The project started in 2010 with TS, and TN joined in 2016. Their scientific objectives are many. About half the observing time is dedicated to the detection and characterisation of exoplanets, the most famous example being the discovery of the TRAPPIST-1 system [32], the other half of the observing time being dedicated to the astrometric and photometric characterisation of small bodies, ranging from MBAs [33] up to TNOs [34], through comets [35].

In terms of specifications, the TRAPPISTs are, by construction, identical mechanically: they are both Astelco lightweight Ritchey-Chrétien telescopes with mirrors of 60 cm in diameter. Their differences lie in their instruments. As we mainly used data from TS, we are only going to enumerate its characteristics.

The TS telescope is a Ritchey-Chrétien lightweight telescope with a German equatorial mount. Being a small robotic telescope is of most importance for its purposes. Such telescope grants less off-axis optical errors in its field of view, making these instruments really competitive for imaging. Its camera is FLI ProLine PL3041-BB with a back-illuminated charge-coupled device (CCD) of 2048×2048 pixels which represents a field of view of $22' \times 22'$. The German equatorial mount, with the polar axis of the mount aligned with the polar axis of the Earth, allows to track automatically targets on the sky. As all German equatorial mounts, to avoid crashing the telescope into the mount, it can perform a meridian flip (a change of 180° in both RA and DEC axes) before continuing to track the target. This creates a gap of a few minutes in the observation and produces a shift in the lightcurve as the stars are no longer located on the same pixels.

Furthermore, we can select some parts of the spectrum of the object by using filters. The telescope is equipped with a double Apogee AI-FW50-10S filter wheel. In total, the two wheels hold 7 broad-band filters (like B, V, Rc and Ic) and 11 narrow-band cometary filters (like OH, NH and CN). From the data we have used, the observations were usually made with the Astrodon I+z or z filters for transiting exoplanets, and the Johnson & Cousins Rc filter for asteroids.

Finally, the TS telescope is equipped with a CCD camera that converts the incident photons arriving on one pixel to a localized charge that will be converted in analog-to-digital unit (ADU). We can define the quantum efficiency (QE) that indicates how many electrons are generated per photon. Furthermore, for fainter targets, we can combine pixels two by two making the detector four times more sensitive. This corresponds to a binning 2 while a one-by-one pixel, i.e. each pixel is considered individually, corresponds to a binning 1. A summary of the characteristics of the TS telescope can be found on Table 2.1.

[17] `https://www.trappist.uliege.be/cms/c_5006023/en/trappist`

	TRAPPIST-South
Site	La Silla Observatory (I40)
Altitude (m)	2315
Coordinates	29° 15' 16.6" (S) / 70° 44' 121.8" (W)
Telescope	Astelco RC Lightweight Ritchey-Chretien - F/8 - 0.6 m
Mount	Astelco NTM-500 - German equatorial
Camera model	FLI ProLine PL3041-BB
CCD type	Back-illminated
Array size (pixels)	2048×2048
Pixel size (μm)	15
Pixel scale (arcsecs/pixel)	0.64
Field of view	$22' \times 22'$
Gain (e/ADU)	1.1
Peak QE (%)	96
Read-out modes (MHz)	1×1 /1×2 / 2×2
Read-out noise (e)	9.5 / 14 / 14
Read-out time (s)	6 / 4 / 2
Dark current (e/s/pixel)	0.11 (at -35°C)
Filter wheel model	Double Apogee AI-FW50-10S
Filters (wheel 1)	B, V, Rc, Ic, Sloan z, I+z, Exo, NaI, H_2O^+
Filters (wheel 2)	OH, NH, CN, C_3, CO^+, BC, C_2, GC, RC

Table 2.1: Table summarizing the TRAPPIST-North characteristics

2.3 Image calibration

The images taken by the telescopes are described as "raw" as we have systematic effects that have to be removed in order to obtain the calibrated images. This is called the calibration. We are not going to discuss this point as the description made by Sicorello in his master thesis is sufficient (see ref [1]).

2.4 Photometry

In this section, we discuss the photometry and lightcurve analysis of asteroids.

2.4.1 Principle

When observing a light source with a telescope, the CCD collects photons that excite the electrons inside the CCD which are collected by the system. Without going into electronic details, an analog-to-digital converter transforms the N electrons that were excited into a number of ADUs according to the gain of the system, expressed in e^-/ADU. The telescopes measures the instrumental magnitude, generally given by the formula:

$$m = -2.5 \cdot \log(I)$$

with I the total intensity of the target, which is computed as $I = \text{ADU} \cdot \text{gain}$.

Instrumental magnitudes are not particularly useful because they are dependant on the telescope (through the number of electrons that are readout, the gain of the system, etc...). However, we can obtain magnitudes that are no longer dependant on the system. This can be done by converting the instrumental magnitudes into apparent magnitudes. The formula needed is the following:

$$m_a = m_i - \kappa X - A + z_P \tag{2.1}$$

where κ is the first-order extinction coefficient, X is the airmass, A is a transformation constant and z_P is the magnitude zero-point. Let us define these quantities properly.

The extinction

When dealing with ground based observatories, the incoming light from the observed source is partially absorbed by the atmosphere: we talk about extinction of the light. This phenomenon is in fact complex as the atmosphere scatters more blue than red light, so the extinction is a function of the wavelength. However, most observations are made using filters so the range of wavelengths that is measured is narrow enough to consider a constant value for the extinction coefficient. We therefore need to have a tabulated value for each filter.

The extinction coefficient, noted κ has units of mag/airmass.

The airmass

The airmass, noted X, represents the quantity of atmosphere between the target and the observer. The airmass is minimum at the zenith and maximum when looking at the horizon. Its value can be approximated by the formula:

$$X = \frac{1}{\cos(z)} \tag{2.2}$$

with z the zenith distance, which is the distance between the target and the zenith (i.e. the point at which the airmass is minimum). It is expressed as: $z = 90° - \text{altitude}$.

The transformation constant and the zero-point

Finally, once the effects of the atmosphere have been levelled, the magnitudes of the objects present in the images need to be re-scaled to match with catalogued values. To obtain them, measurements of reference stars are made with each filter. The magnitude that is obtained has to be shifted by z_P to match the tabulated value, and thus the zero-point is obtained.

Note that in the literature, it is possible to find the transformation constant (A) and the zero-point (z_P) combined into one single value, simply noted z_P.

In formula 2.1, the instrumental magnitude is computed by the `ssos Pipeline` (see Chapter 3), the airmass is found in the header of each image, the transformation constant is set to be -25 for TS. However, the extinction coefficient and zero-points need to be tabulated for each filter. They are calculated by the TRAPPIST team and are recalled in Table 2.2.

Filter	Wavelength λ (Å)	Extinction coefficient κ (mag/airmass)	Zero-point z_P (mag)	Zero-point error σ_{z_P} (mag)
OH	3090	1.60	7.005	0.044
NH	3362	0.65	6.552	0.039
CN	3870	0.36	5.994	0.019
C_3	4062	0.36	5.963	0.017
CO^+	4266	0.25	5.846	0.043
B	4440	0.25	2.631	0.014
BC	4450	0.25	6.170	0.006
C_2	5141	0.15	5.223	0.005
GC	5260	0.14	6.175	0.007
V	5483	0.14	2.752	0.007
NaI	5890	0.13	6.585	0.000
Exo	6000	0.10	1.370	0.000
Clear	6000	0.07	2.000	0.000
Rc	6855	0.098	2.543	0.008
Ic	8637	0.043	3.177	0.010
H_2O^+	7020	0.07	5.000	0.000
RC	7128	0.05	6.668	0.012
I+z	9000	0.07	3.000	0.000
z	9200	0.07	3.000	0.000

Table 2.2: Values of the extinction coefficient, zero-point and zero-point error for each of the 18 filters of TS calculated by the TRAPPIST team. We recall the approximate wavelength that is used. The "Clear" filter corresponds to an observation made without any filter.

2.4.2 Differential photometry

A more advanced way to perform photometry is through differential photometry. In this case, we do not only consider our target but also comparison objects. The idea is to subtract the average magnitude of comparison stars (non-variable) from the target magnitude. By doing so, we remove as much systematic variations as possible, like clouds passing in front of the target or variations in atmospheric conditions. Ideally, we should take as much comparison stars as possible, but close to the target (to have the same atmospheric effects) and with spectral types close to the target (to avoid different extinction effects for different lights). When dealing with asteroids, the light we measure is the reflection of solar light and the comparison stars should have a spectral type close to the one of the Sun.

Differential photometry was added to the pipeline with the use of the `Photometry Pipeline`. In our case, we use a minimum of 3 comparison stars with solar-like colors (see Chapter 4).

2.4.3 Lightcurves

Once the magnitude of the object as a function of time is computed, we obtain its lightcurve by plotting it. As asteroids are spinning, we measure variations in their lightcurves due to the variations of the illuminated area that is shown to us. Depending on the rotation speed of the asteroid, one observation could be enough to measure a full period. If it is not the case, we would need more than one observation to be able to reconstruct its full period. Furthermore, having longer observations allows to have multiple periods which increases the quality of the period determination, and also limits the effect of aliasing[18].

Furthermore, asteroid lightcurves can also give information on their shapes. By taking lightcurves of the asteroids at various phase angles[19], we can use a lightcurve inversion method to reconstruct the 3D shape of the object [36, 37].

In this work, we will limit ourselves to the period determination from one or multiple pieces of the lightcurve depending on the number of detection of the same asteroid.

[18] An alias is a multiple of the true period.

[19] The phase angle is the angle between the incident and the reflected light of an object. A varying phase angle of an asteroid means we observe it from a different angle and see another part of it.

Chapter 3

The `automated SSOS pipeline`, Part 1: `ssos`

In this chapter, we present the `automated SSOS pipeline`. This corresponds to what our predecessor, Sicorello, has been working on during his own master thesis during the academic year 2019-2020. In the following pages, we recall the state of the art and what were the improvements we made.

3.1 Overview of the pipeline

The idea behind the design of the `automated SSOS pipeline` appeared with the project of Malkhe et al. (2019): the `ssos Pipeline` (hereafter `ssos`) [38], which itself was build from the Kilo-Degree Survey (KiDS) pipeline from Malhlke et al. (2018) [39]. In short, it is a tool which filters the sources between each astrophysical image in order to extract moving objects.

As half of the time of observation of the TRAPPIST telescopes is dedicated to the study of asteroids and the other half is dedicated to the observation of transiting exoplanets, we can get the best from both of these worlds. Indeed, when looking into the ecliptic (when observing asteroids), we can extract multiple known asteroids per field, whereas when looking outside of the ecliptic (when observing transiting exoplanets), we have fewer known asteroids and thus a higher chance of discovering a new one.

We have to keep in mind that we have two types of data. We have fresh data that is produced by each telescope each and every night which needs to be processed as soon as possible. Indeed, discovering a new object is a race with other facilities. The second type of data is all the past observations that have been collected. We have years of images, around 10 for TS and 5 for TN, that are archived and that certainly contain unknown objects. Therefore, the pipeline needs to be built in a way to allow the processing of both data sets.

This is the philosophy behind `ssos`. But in order to run it, the data needs to be prepared, meaning that the compressed and raw data coming from the telescope has to be decompressed, sorted, calibrated, processed and the outputs need to be accessible, readable and useful. This is the automated part implemented by Sicorello.

The first version of the pipeline was divided into 5 main steps:

1. pre-processing and pre-sort: the raw and compressed images of the night are copied to a different folder in which they are uncompressed. They are then sorted following the binning and the readout mode that were used during the observation;

2. calibration: the raw images are calibrated using `PyRAF`[20], a `Python` script for Image Reduction and Analysis Facility (IRAF). During this step, the pipeline automatically makes use of the calibration images, the flat, bias and dark images, in order to calibrate the data;

3. post-sort: once the images are calibrated, they are almost ready to be used for a scientific purpose. However, during a night of observation, a telescope generally observe multiple fields, i.e. multiple targets. This means that we need to sort again the images according to the science target;

4. `ssos`: once every folder are properly sorted, the pipeline launches its most important function: `ssos`. Here, as everything is already coded, we only tweak the parameters to adapt them to the telescope(s) we are using;

5. cleaning the drive: once `ssos` has been launched successfully, the pipeline deletes the raw and calibrated folders in order to not saturate the hard drive with data that is no longer necessary.

3.2 `ssos` in more details

As it is the most important part of the pipeline, we dedicate this section to the description of `ssos`.

The pipeline automatically searches for serendipitous asteroids in astronomical images through the use of filter routines. But first, the sources present in each images are extracted with SExtractor (Source Extractor) [40]. The idea is to associate the pixel data to a catalogue data: a photon impacting the CCD on a given pixel (x,y) can be linked to a source located at a position (RA,DEC) in the sky. Once all sources have been extracted in each images, they are associated to real sources through the use of SCAMP [41]. Once this step is done, we obtain a catalogue that lists all the sources detection of all images (full_1.cat) which contains all the known stars in the field, but also contains source detection of cosmic rays (CRs) and potential traces left by serendipitous objects. The heart of `ssos` is the proper filtering of real moving objects (asteroids) from non-moving objects (stars, galaxies, hot pixels...) and random detections like cosmic rays.

To perform its duty, the pipeline relies on any combinations of up to 6 different filters:

1. number of detections: this filter is plain and simple, we simply retain sources that are detected more than N times. This allows to remove all the CRs detection that does not stay on the CCD for more than 2 or 3 images. In the default version of `ssos` (not the default version of this pipeline) this filter is set to True and the number of detections is set to 3. However, we set up the number of detections to 10 in order to drastically reduce the number of false-positives, as two filter and subfilter were deactivated (see below);

[20] `https://github.com/iraf-community/pyraf`

2. proper motion: this filter looks at the relative speed of the source. As we search for solar objects, their relative speeds range from close to 0"/h for the most distant KBOs to a few 100"/h for the NEAs. This filter removes all the sources that have a relative speed outside of this interval. In the default version of `ssos`, this filter is set to True with relative speeds in the range [0;300] (expressed in "/h). Moreover, it also looks into the signal to noise ratio (SNR) of the proper motion, meaning we calculate the ratio between the absolute value of the proper motion and its error. A real SSO will display a rather large proper motion and will therefore have a greater SNR. On the contrary, a non-SSO will display a rather small proper motion and will therefore have a smaller SNR. In the default version of `ssos`, the value of the SNR is set to 0.5. We kept the default parameters of this filter;

3. pixels: this filter removes the hot pixels that could be left present in the images even after calibration. Such pixel will be considered as a source on all the images. However, as it stays at the same position on each image, it can be easily identified by the pipeline. This filter therefore looks at how many pixels the source has moved during the observation to discriminate it from a hot pixel. In the default version of `ssos`, this filter is set to True and the distance in pixels is set to 2. We kept the default parameters of this filter;

4. motion: this filter is similar to the proper motion one in the sense that it also looks into the physical motion of the source. In this case, we look into how straight the motion of the source is. This filter works by measuring the χ^2 of the motion. A true straight line displays a value of 1, and the farther we are from this value, the less straight the motion is. In the default version of `ssos`, the filter is set to True and the χ^2 value is set to 0.95. However, the linear fit can be fooled by larger data sets. This filter therefore has a subfilter that tries to separate the detection in multiple ones if there is a gap in the detection longer than a set value. This threshold is expressed in units of median absolute deviation (MAD) and is set to 1.5 in the default version of the pipeline. We kept the default parameters of this filter;

5. trail: this filter looks at the shape of the source. Indeed, SExtractor consider each source as an ellipse of semi-major axis a and semi-minor axis b. From image to image, we expect the shape of the source to vary slightly, but a real object should keep its general shape. The discrimination performed by this filter follows the value of the ratio between the average weighted uncertainty and the standard deviation of the data. A small ratio allows for strong variations in the shape of the ellipse, and the pipeline filters all the detections that are bellow this value. Note that it is computed for both axis. In the default version of the pipeline, this filter is set to False because it is extremely strict, even with the default value of the ratio set to only 0.25;

6. bright sources: bright sources are stars that saturate the images. They pollute the region of the CCD around them, so this filter ignore all detections in a given radius around such bright stars. In the default version of the pipeline, this filter is set to True, the distance from the bright sources is set to 200", the bright sources themselves are taken from the HYG Database[21] and the limiting magnitude are -99

[21] `http://www.astronexus.com/hyg`

FILTER_DETEC	True
DETECTIONS	10
FILTER_PM	True
PM_LOW	0
PM_UP	300
PM_SNR	0.5
FILTER_PIXEL	True
DELTA_PIXEL	2
FILTER_MOTION	True
R_SQU_M	0.95
IDENTIFY_OUTLIER	True
OUTLIER_THRESHOLD	1.5
FILTER_TRAIL	False
RATIO	0.25
FILTER_BRIGHT_SOURCES	False
BRIGHT_SOURCES_CAT	REFCAT
DISTANCE	200
MAG_LIMITS	-99,99

Table 3.1: Table listing the parameters we used for each filter.

and 99. In our version of the pipeline, the catalog that is used is REFCAT, the reference catalog of SCAMP, but the filter was deactivated.

A summary of our parameters can be found on Table 3.1. As the filtering is dependant on the sources extracted by SExtractor, we discuss our parameters in more details in Section 3.6.

3.3 `ssos` outputs

We now describe all the outputs produced by the `ssos` part of the `automated SSOS pipeline`.

As `ssos` is launched for each field, it can run multiple times on a given night. For each field, the outputs are saved in a unique folder that can easily be accessed by the operator. Such output folder contains in fact 7 subfolders (5 by default but we also have subfolders containing the lightcurves of the retrieved objects and a statistics of the detection). The subfolders are described here bellow:

1. cats: this subfolder contains various useful files. It takes its name from the various catalogues that it contains. We only mention the three that are always of use. First, we have the full_1.cat produced by SCAMP. It contains all the sources detected on all the images with their positions. We use it every night to quickly check if we have traces of a SSO in the field. The second catalogue is named skybot_all.csv. It is produced by SkyBoT [42] which checks in its database if there are known SSOs in each image. Therefore, this file contains, among other, the name, positions and

magnitudes of each known object in each image. The third and last very useful file is the ssos.csv file. Each time the pipeline is ran, it produces this output file. It contains more or less the same info as the SkyBoT file, but here we list the retrieved objects. That means that we can have already known objects for which we retrieve their position and magnitude, but it can also list newly discovered objects;

2. checkplots: the checkplots are an optional analysis that can be performed by `ssos`. This option is not used as we trust the recovery of known asteroids performed by the pipeline;

3. cutouts: this subfolder is also of a paramount importance in `ssos`. It contains the so-called cutouts of the retrieved objects: squared images with the source in the middle. The operator can easily type a command in the console to open these cutouts that appear as a GIF on the screen. It can then approve the objects as a real asteroid or reject it with the press of a key;

4. lightcurves: this subfolder contains two types of files, the txt and the png of the lightcurves of each of the objects that were retrieved by `ssos`. This is particularly useful to check if the known objects that were retrieved have good lightcurves and for the unknown objects, the appearance of the lightcurve can give clues to the quality of the detection;

5. logs: the subfolder simply contains the log file of `ssos`. If the night needs to be processed more than one time, because the operator needs to fine-tune the filters in order to retrieve a known asteroid, another log is added here;

6. statistics: this folder contains a text file that is an addition to the outputs of `ssos`. A small routine summarises the detection by precising if an asteroid was recovered or not;

7. weights: the folder contains weights files that can be used by SExtractor when extracting the sources. Such option is not used in the pipeline process, and this subfolder is therefore empty.

3.4 The role of the operator

In this section, we briefly describe the function of the operator as it was expected in the first version of the `automated SSOS pipeline`. The general actions that need to be made are as follow:

- we consider here that the pipeline is ran manually on the computer of the institute, which means that the fresh and raw data must be manually transferred to the computer;

- the operator can launch the pipeline on the night coming from the telescope with the use of the command:

```
$ ./start.sh <telescope_id> <observation_night>
```

- once the pipeline has finished, the operator needs to manually check each output individually:
  - the ssos.csv file listing all the detected objects, which needs to be compared to the statistics of the detection to judge its quality;
  - the full_1.cat file which needs to be open with TOPCAT[22] in order to manually plot the position of all the sources in the images in (RA,DEC) space. This is done to check for traces potentially left by the sources and to cross check their positions with the ssos.csv file;
  - to look at each lightcurve individually. Indeed, although the lightcurves themselves are not fully reliable, they can nonetheless offer a quality check of the recovery;
  - to access the cutouts via the command inside the output folder:

    ```
    $ ssos --inspect ./
    ```

    and manually confirm or reject the detection of each recovered source;
  - finally, the MPC report can be build via the command:

    ```
    $ ssos --mpc path/to/output/csv
    ```

In summary, the `automated SSOS pipeline` had room for improvements in order to reduce the number of human actions that are needed in order to build the final output: the MPC report. Furthermore, the quality of the filtering could be improved and some optimisations could be made.

3.5 New additions to SSOS

In this section, we present all the new functions and improvements relative to the `automated SSOS pipeline`.

3.5.1 Outputs

The first version of the `automated SSOS pipeline` let the operator travel to the general output folder, where it needed to check various files in order to obtain various information. We decided to build a single PDF file containing all these information. This PDF file contains a small text giving info on the observation itself and it contains one image per page so they are easily readable. It is built as follow:

- a short list, present on all pages, recalls the telescope that was used, the date and time of the first and last images, the airmass at the start and end of observation, the scientific target, the target (RA,DEC), the number of images, the filter, binning and exposure time, and finally the path to the output folder. The idea here is to have all the information relative to the observation itself. The target name and position (in other words, the center of the field) inform us on where we are looking (in the

[22] `http://www.star.bris.ac.uk/~mbt/topcat/`

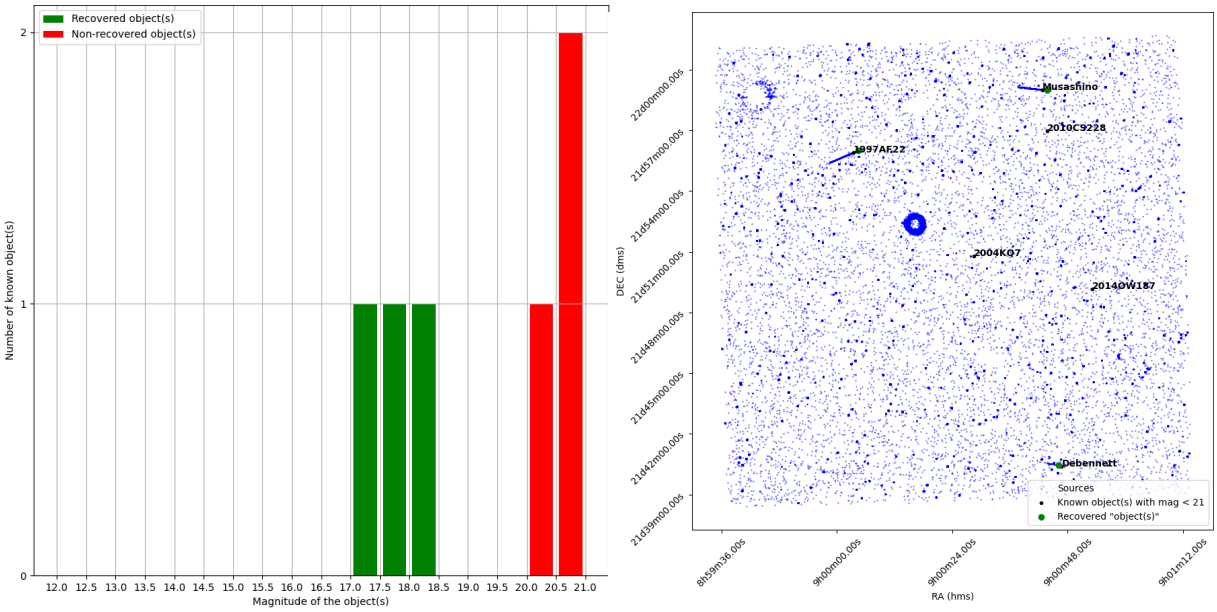

Figure 3.1: The first two figures that are available in the PDF summarising the night (here the field of the star SP0900+2150 observed during the first half of the night of March 9th, 2020 by TS). On the left, we have the histogram of the detection, counting the recovered asteroids in green and the non-recovered ones in red. The magnitudes range from 12, the brightest asteroids, up to 21, the limiting magnitude. On the right, we have the traces of the sources extracted by SExtractor, in (RA,DEC) space, with the names of the asteroids retrieved by SkyBoT (in black) and the sources that were recovered (in green). Notice that 3 asteroids left straight traces on the plot, and all three are recovered as it confirmed on the previous histogram. The remaining three asteroids are too faint to leave traces and be recovered. The two donuts shape that are visible on the upper left quarter of the plot are dust features that were not properly flat-fielded during calibration of the images.

ecliptic or away). The airmass is not particularly necessary but it can give clues to a low quality lightcurve that was obtained at very high airmass;

- on the first page, we have an histogram that is important for checking `ssos` performance on the field. It plots the number of known asteroids that are recovered and those that were not (see the left panel on Figure 3.1). This allows to check in an instant if `ssos` recovered all the obvious objects. By "obvious", we mean asteroids that are bright enough. Depending on the filter, binning, exposure time and atmospheric conditions, the limiting magnitude will vary;

- the second page contains the visualisation of the full_1.cat file, meaning we plot the traces of all sources. Therefore, we no longer need to open the full_1.cat with TOPCAT and to plot the positions of the sources in (RA,DEC) space manually. An important information we added is the position of all known asteroids in the field, plus the positions of all the recovered objects (see the right panel on Figure 3.1). This way, there is no longer the need to open another file to manually check the position of the recovered objects in the plot (which was tedious). This is extra useful

as we can easily see if there are traces that are not recovered, or if the recovered sources which are unknown are leaving traces;

- the following pages contain the lightcurves of all the recovered objects, real or not. For known asteroids, the operator can check if the lightcurves are of quality, meaning if the magnitudes and the errorbars are realistic. For unknown detection, it can give further clues to the reality of the object.

With the addition of the PDF, the operator only needs to launch the pipeline, check this file, open the cutouts and build the MPC report. The human time required has been decreased whereas the ergonomy and quality of the judgements have been increased. An example of such PDF report can be found in Appendix B.

3.5.2 Other improvements

Other improvements have been made to the pipeline.

First, the pipeline is expected to run on the data coming from both TRAPPIST telescopes. In its first version, only TS was fully supported, now, it can also be ran on data coming from TN.

Second, we applied the formula to convert the instrumental magnitudes provided by `ssos` into apparent magnitudes in order to have better lightcurves. Speaking of which, the lightcurves themselves have been improved by tweaking the SExtractor parameters (see below) and by adding the meridian flip on the relevant plots. Moreover, the time axis is also more readable, the start (resp. end) of the graph being at the start (resp. end) of the observation. This allows to have a better opinion of the detection for the asteroids that are visible for a fraction of the total duration. A side by side comparison of a past and new lightcurve can be seen on Figure 3.2.

Third, we made several optimisations. The more important and more relevant are related to `ssos`. We replaced the SExtractor configuration files with updated ones and the parameters of the `ssos` configuration file have been refined. This is discussed in the next section.

Finally, we have also been working on a user guide. As we were discovering the pipeline after a year of work by Sicorello, we thought it was a good idea to document our own experience with this tool. This way, future users have a reference that they can use if they have any questions, and they can edit the guide if the pipeline is modified in the future.

3.6 To filter or not to filter?

In this section, we discuss the filter parameters that were chosen. We will use Table 3.1 as a reference. We recall that the 6 filters offered by `ssos` are discriminating each source extracted by SExtractor, this means that the work of the latter is the bottleneck of the filtering quality.

In the work of Mahlke et al. and in the default version of `ssos`, only the strongest filter, FILTER_TRAIL, was deactivated. Indeed, it rejects known asteroids and the 5 other filters were enough to provide robust outputs with few false-positives. Depending on preferences, it is possible to choose more strict or loose parameters in order to modify the

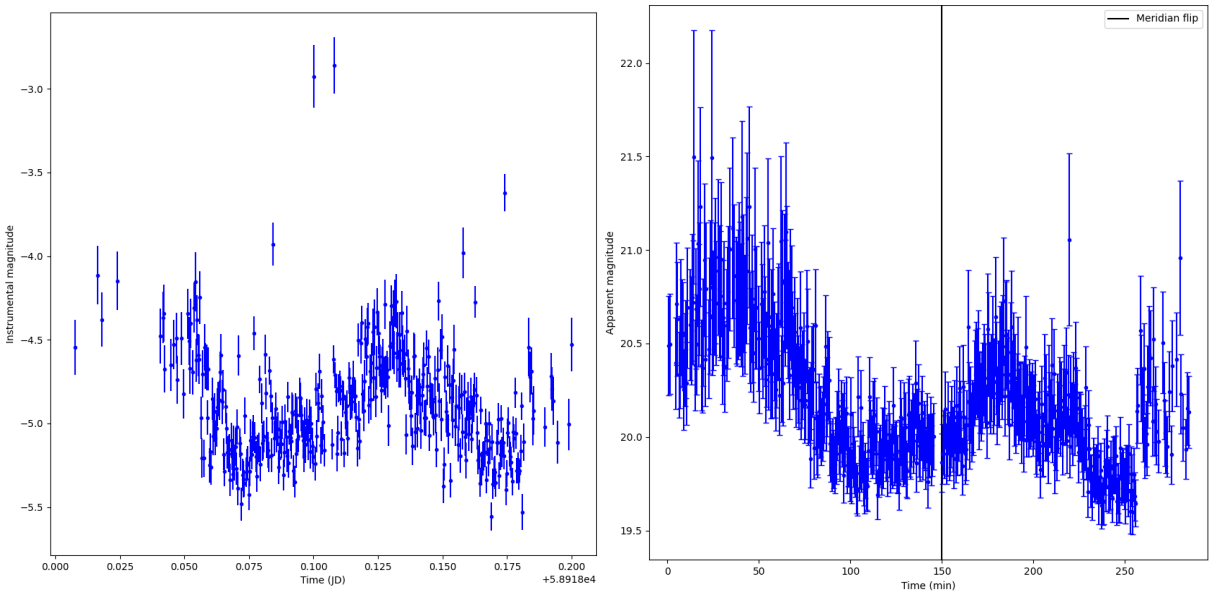

Figure 3.2: Side by side comparison of the same lightcurve obtain with the old parameters (left) and the new (right). The meridian flip is indicated and the detection is more pronounced at the beginning of the observation. These lightcurves correspond to the MBA (3249) Musashino retrieved on the night of March 9th, 2020.

filtering. We could choose to have a very loose filtering at the cost of some false-positives, or the opposite, a very strict filtering at the cost of a few misses of real asteroids.

We recall that the BRIGHT_SOURCES filter was also deactivated. We did not like the idea of ignoring entire regions of the CCD (with a radius of 200" by default, this corresponds to a radius of 312.5 pixels for TS) and we preferred working on each source individually. We also added initially a slight decrease of the filtering with the deactivation of the INDENTIFY_OUTLIER subfilter. This choice is acceptable because we can lift a filter as long as we increase the filtering of the remaining ones. The balance was reestablished with an increase of the DETECTIONS parameter from 3 to 10. Indeed, most remaining false positives were only detected a few times.

Let us now discuss our parameter choice for each filter individually.

First, the detection filter. It is, in our opinion, a mandatory filter, as a real object needs to be detected on at least 3 images to be confirmed, but we decided to set the constraints on the detection to have at least 10 points. This value seems to be satisfying as all the detections we obtain with our set of parameters have much more than 10 points. Furthermore, the more points we have, the easier it is to confirm or reject a detection, which is much harder with the minimum of 3 points. However, we note that for the known comet observations of the TRAPPIST survey, we have less than 10 images, usually only 4 in R band (by design of the observing strategy) and thus a filtering of all sources. The pipeline was not modified to accommodate for such case as SkyBoT does not take charge of comets.

The second filter, the "pixel" one, is also mandatory. As a real asteroid travels always more than 2 pixels in total, this little routine allows to filter only bad pixels and is therefore not detrimental to the recovery of real objects.

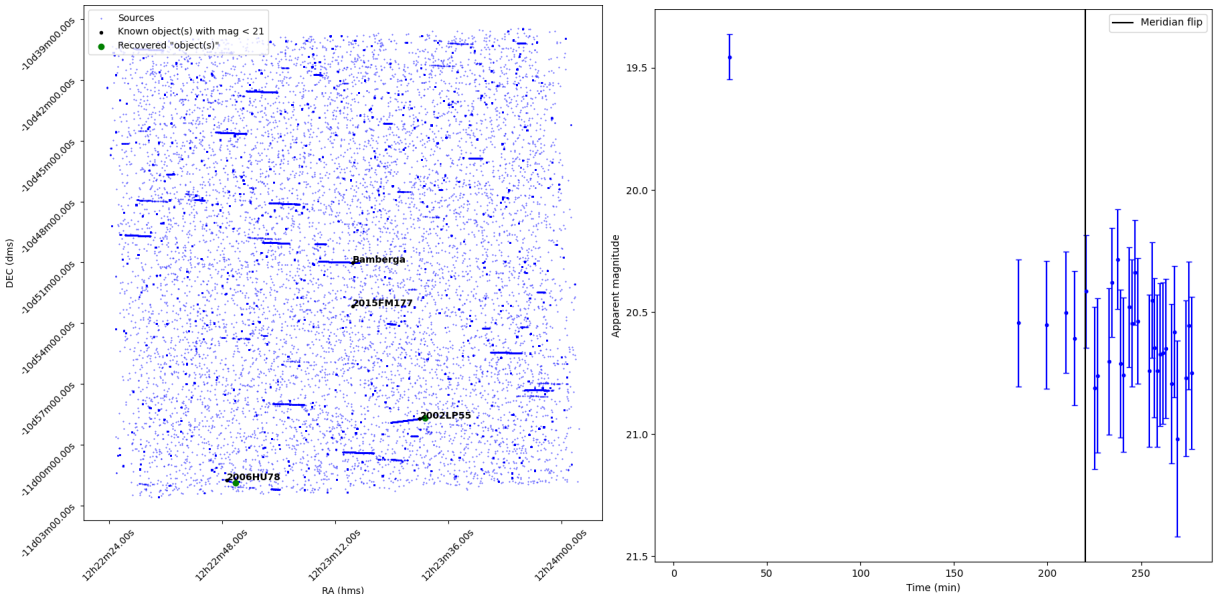

Figure 3.3: Left: example of the bright asteroid (324) Bamberga not being recovered by the pipeline. The streaks parallel to the trace of (324) Bamberga are due to hot pixels that were not removed during calibration. The plot was obtained processing the night of February 19th, 2020 (TS). Right: typical false positive that is obtained with the IDENTIFY_OUTLIER subroutine deactivated. By having it on, the single detection is separated from the larger group. The two new groups need to pass the filters, which is sufficient to often remove this type of detection. This false-positive was retrieved on the night of March 18th, 2020, during an observation of TOI736 with TS.

We now discuss the motion filter, the one relative to the linearity of the motion. It is the most tricky to adjust. From the results we obtained, we found that for the brightest asteroids from the MAB, at around mag 12 to 14, the filter was rejecting the detections. We tried lowering the χ^2 parameter but only deactivating the filter seemed to work. As the other three are rather weak, deactivating this one left us with dozens of false-positives so keeping it off was not acceptable. However, a temporary solution for the few cases that pose problem is the fourth filter relative to the proper motion. Indeed, this one is extremely robust and flexible. As SkyBoT gives us the relative speed of known asteroids, it is possible to narrow the range PM_LOW and PM_UP when deactivating the motion filter. Now, one might think we could miss a bright but unknown asteroid due to this filter. Indeed, the current set of filters would not recover the unknown object, but it will leave a clear trace on the relevant plot of the summary, and thus the operator would clearly see it by eye (see the left panel of Figure 3.3). In such case, the pipeline would have to be ran once again to recover the bright asteroid filtered by the motion filter.

Finally, we found that we usually had a few strange detections in the sense that we often had a train of detections with another source linked to it at the beginning or the end of the observation (see the right panel of Figure 3.3). We understood that such outliers could be removed with the proper subfilter and thus we reintroduced IDENTIFY_OUTLIER with its parameter OUTLIER_THRESHOLD to its default value of 1.5.

We therefore use four filters: detections, proper motion, pixel and motion. Indeed, 10 detections is a minimum to confirm that we have a real object. The pixel filter is the

	Mahlke et al.	Us
DETECT_TYPE	CCD	CCD
DETECT_MINAREA	5	5
DETECT_MAXAREA	0	0
THRESH_TYPE	RELATIVE	RELATIVE
DETECT_THRESHOLD	1.5	1 / 1.2
ANALYSIS_THRESHOLD	1.5	1 / 1.2
DEBLEND_NTHRESH	16	32
DEBLEND_MINCONT	0.05	0.005
CLEAN	Y	Y
CLEAN_PARAM	1.0	1.0

Table 3.2: Table comparing the SExtractor parameters relative to the extraction of sources used by the default version of `ssos` and our current version of the pipeline.

weakest and not removing a lot of sources. The proper motion filter is the most flexible. The motion filter, even though it poses problems, remains the strongest and deactivating it would leave us with an unbearable number of false-positives.

An important thing to understand is that the filtering is performed on the sources extracted by SExtractor. Therefore, its proper configuration is mandatory to guarantee the optimal filtering, or else the filters serve no purpose.

We thus decided to update the parameters of SExtractor relative to the source extraction. Such parameters can be found on Table 3.2.

The first parameter is linked to the detector that is used, here a CCD. The following two defines the number of neighboring pixels that define a detection, here we need at least 5 to have one and we have no upper limit. The fourth parameter specifies that the detection threshold is expressed in σ above the noise.

The most important change that was performed is relative to the threshold parameters. The detection and analysis thresholds were reduced from 1.5σ to 1σ above the noise, which allows the extraction of fainter sources. This effect could be reinforced by deactivating the cleaning process of SExtractor. It is supposed to remove sources that are not linked to astrophysical sources and although removing it gives us more sources to work on, their relevance is debatable and thus we decided to keep it on as lowering the threshold was sufficient. Note that the more sources are extracted, the more computing time is needed. Using the default value of SExtractor of 1.2σ for the detection and analysis threshold could be better suited when processing a large amount of nights. This is not a problem when dealing with a single night (see Figure 4.2 in Chapter 4).

Finally, we decided to crank up the deblending performed by SExtractor. The principle is the following. Two different stars that are close enough could form one packet of bright pixels. SExtractor can try to deblend them to have two distinct sources related to the two stars. This is linked to the DEBLEND_NTHRESH and DEBLEND_MINCONT parameters. The values we chose are the ones used by default by the SExtractor.

3.7 Remaining matters

To conclude this chapter dedicated to `ssos`, we briefly cover the remaining matters that are posing problems or that can still be improved.

In order to have a pipeline that works on 100% of the fields, adapting it to run on the observation of the comets is going to be necessary. As we wrote previously, comets are usually observed with less than 10 images taken, which means that in the current state of the pipeline, no sources are ever going to be extracted. This could be easily updated by checking the number of images before running the pipeline and automatically changing the corresponding parameter accordingly. However, a thorough update would be harder. Indeed, such observations are made with various filters to study in detail the coma, which means that we would also have to accommodate for the changing filters when `ssos` performs the photometry. For now, this matter is left as-is, but comet related fields could have potential as the exposure time are quite long and could thus reveal faint and small unknown asteroids.

Another problem we encountered is related to the apparent magnitudes we compute. Indeed, they are about 1 mag above what we expect, meaning the asteroids are much fainter than in reality. We currently have no explanation for such a huge discrepancy. To add to this unsolved matter, the apparent magnitudes are computed using Equation 2.1 (see Chapter 2), which relies on calibrations that are regularly made by the TRAPPIST team to update the zero-points. Even though the integrity of the telescope is not drastically changing with time, calibrations made in 2021 are nevertheless not perfectly adapted for observations made in 2010.

On a similar topic as above, calibrations are not always perfect either. We often have dust particles that are still visible (see Figure 3.1) or hot pixels that leave traces similar to the target when observing moving objects (see left panel of Figure 3.3). Furthermore, the calibration images are not taken every night and we thus use older calibration images. In summary, the calibrated images are not always clean which could slightly impede the pipeline to retrieve some asteroids[23].

[23]The calibration that are taken must be older ones. This is logical when processing fresh data, but it is recall nonetheless when processing older data, as we can "go back" in time. A proper way to deal with past data would be to start at a given date and "advance" in time.

Chapter 4

The automated SSOS pipeline, Part 2: PP

In the following chapter, we present the Photometry Pipeline (hereafter PP) and how the differential photometry and the extraction of variable stars present in the fields were implemented into the automated SSOS pipeline.

4.1 Overview of the pipeline

In order to perform precise lightcurve analysis, the automated SSOS pipeline was missing a non negligible aspect: differential photometry. This was added via PP, which was developed by Mommert (2017) [43]. This pipeline works in a similar fashion as ssos, but its goals are different. They both use SExtractor and SCAMP to extract and register each source in each image. The difference is that ssos discriminates moving objects from other sources, whereas PP compares its extracted sources to known catalogues in order to perform differential photometry on relevant objects. Thus, PP performs its photometry blindly on already known coordinates.

We describe below the five functions of PP we have implemented into the pipeline:

1. pp_prepare: this first function edits the header of each image in order to make sure everything is compatible for the rest of the pipeline. During this process, PP introduces fake World Coordinate System (WCS) in the header of the images for better image registration. This allows the pipeline to be ran on all images whereas ssos cannot be ran on images that are missing their WCS and which are discarded;

2. pp_register: this function performs both the source extraction (using pp_extract) and astrometric matching using SExtractor and SCAMP in a similar way as ssos. This process is either ran once if all the images have been registered properly, or twice with the prior knowledge of the first registration;

3. pp_photometry: this function builds a curve-of-growth for the moving target and the average of the backgrounds sources in order to minimise the effect of trailing. This is done by calling the pp_extract function with a list of 20 different aperture radii. The best aperture radius is the one for which both the flux of the target

and the background flux are greater than 70% of their total and the one for which the difference between the normalised target and background flux levels is smaller than 5%. After that, pp_extract is launched once more to derive the instrumental magnitudes for all sources in the field, using the previously obtained aperture radius;

4. pp_calibrate: once the instrumental magnitudes are obtained, this function is launched in order to transform them into apparent magnitudes. The calibration is performed directly by the pipeline itself through the use of a reference catalogue and not through the use of parameters like we did with `ssos`;

5. pp_distill: finally, once the calibrated magnitudes are obtained, the pipeline extracts those relative to the target.

4.2 PP outputs

Strengths of PP lies in its robustness and versatility. The former is guaranteed through the use of pp_prepare to make sure that each image can be processed and through the multiple uses of SCAMP to register the sources. The latter is guaranteed through the various options that each functions offers.

The two functions that we configured are pp_calibrate and pp_distill. The calibration process can be performed with only solar-like colored stars, as small Solar System objects are reflecting solar light. We thus avoid any extinction effect that could differentiate photons of various wavelength. Furthermore, the magnitudes can all be converted into a given band, and we decided to force the conversion to the R band by default. This way, there is no need for manual conversion for the multiple filters that are available on TRAPPIST. Furthermore, we noticed that PP was not always calibrating the magnitudes for the asteroids that were directly observed. This happened when the target was very close to saturation. This problem was solved with a tweak in the parameters of the pp_calibrate function.

The pp_distill function allows to extract the magnitudes of serendipitous asteroids and of variable stars present in the field. We stress that the operation of PP is different from `ssos`, as PP runs blindly on previously known coordinates. This is not a problem for the variable stars and the bright asteroids, but it has its limits for fainter objects. In the same manner as `ssos`, it does so by querying the SkyBoT database and comparing it with its own source catalogue. PP extracts the asteroids that have their positions matching the database within 5 pixels and if they are brighter than 90% of the sources in the field. As such, the faintest asteroids are not extracted. For variable stars, PP compares its sources catalogue to the International Variable Star Index (VSX) catalogue[24] to identify all the variable stars and extract their lightcurves.

Note that by default, PP generates its outputs in a file called "diagnostics.html". This was problematic on multiple level. First, each function creates a significant amount of diagnostics, and creating the file accounts for around 20% of the processing time of PP. Second, the visual outputs are available only through this file, which is not ergonomic. We decided to deactivate this part of the pipeline and produce the relevant outputs ourselves. All the outputs of PP are sent into their own "photometry" subfolder directly inside the

[24] `https://www.aavso.org/vsx/`

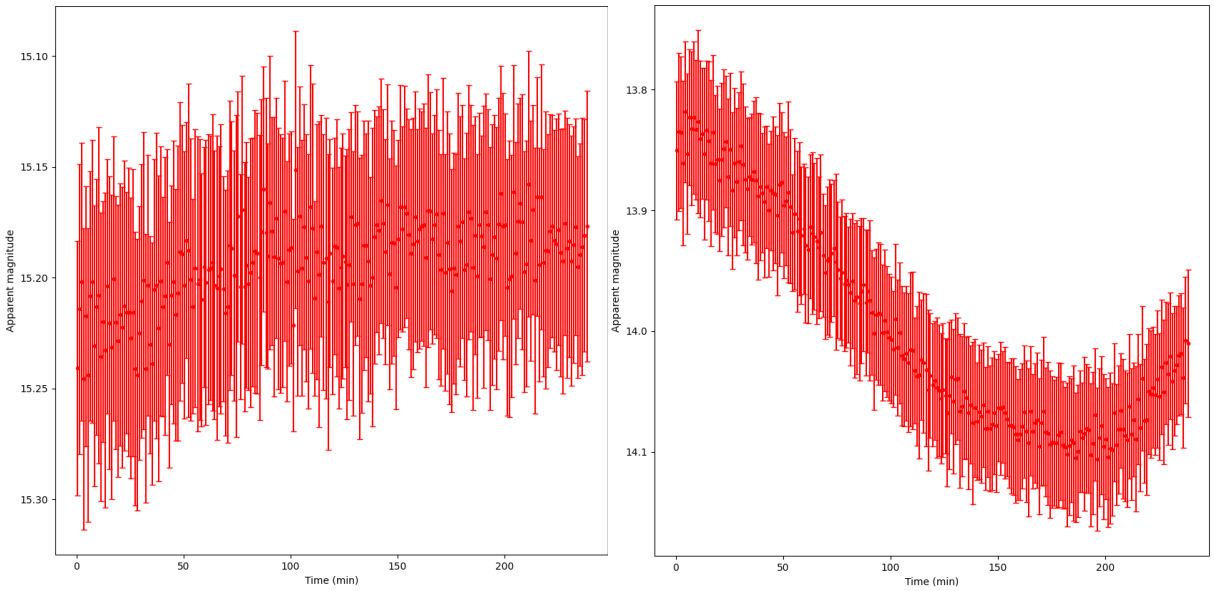

Figure 4.1: Left: example of the lightcurve of the control star performed by PP. The flux is almost perfectly constant throughout the night. Right: lightcurve of the asteroid (208) Lacrimosa performed by PP. It was one of the targets of TS on the night of March 18th, 2020.

output folder of ssos. The lightcurves are all added to the PDF summarising the night after those of ssos for each field. Note that PP generates the lightcurve of a sufficiently bright star that is present in both the first and last image. This allows to have a quality of the photometry that is performed. This lightcurve is always the first that is displayed for clarity. An example of the output of PP can be found on Figure 4.1.

4.3 The photometry pipeline inside the automated SSOS pipeline

From the overview of PP, one notices the similarities in its operation compared to ssos: both use SExtractor to extract the sources in each image, both use SCAMP in order to perform the astrometry of these sources and both goes through the instrumental photometry of the extracted sources. In principle, PP could start with pp_calibrate directly on the instrumental magnitudes provided by ssos. In practice, tweaking the respective SExtractor and SCAMP parameters of both pipelines in order to run PP on the ssos catalogues is no easy task.

In order to explore this possibility, we compared in details their final output catalogues. Those of ssos are much more oriented on the astrometry of the sources, whereas those of PP are more oriented on the photometry. Editing the setup of ssos to allow PP to be run directly afterwards or editing the setup of PP to allow it to run after ssos was abandoned as it would have requested to drastically alter the code of one or the other without any guarantee of success. A second possibility we considered was to keep both pipelines as they are, but adding a routine in between to make the catalogues compatible and allow a smooth transition. Unfortunately, our artificial catalogues were missing information

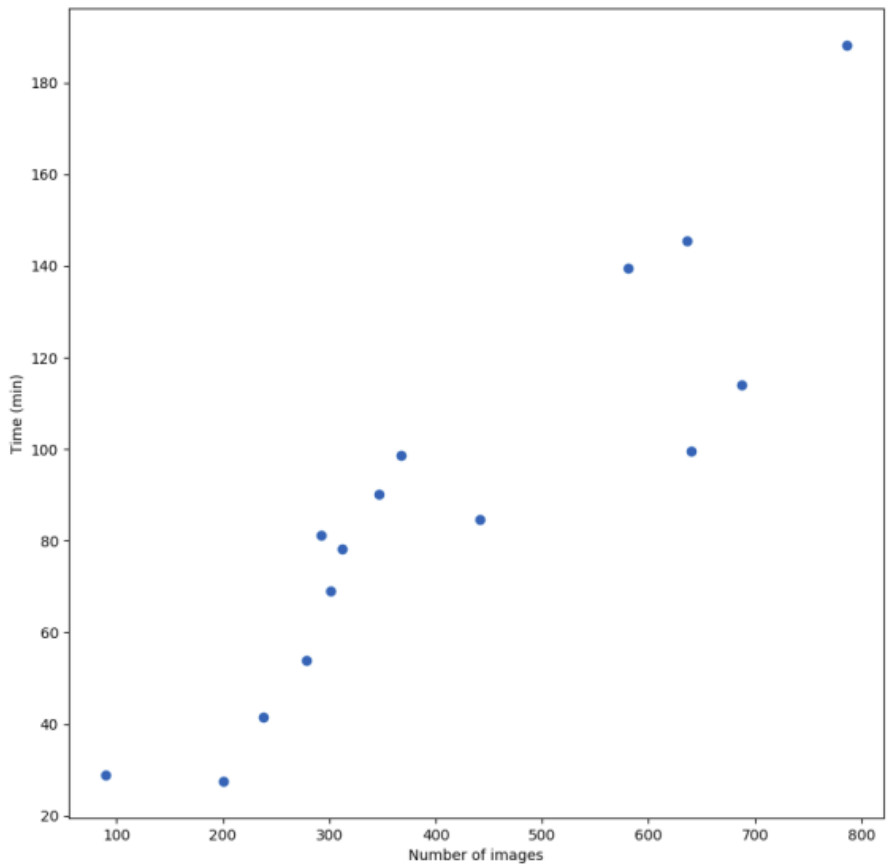

Figure 4.2: Time required by the `automated SSOS pipeline` to process a night as a function of the number of images.

needed by `PP` and thus it could not be run on those.

As we did not find a proper way to merge the pipelines, in the current version of the `automated SSOS pipeline`, both `ssos` and `PP` are run independently, and we will justify this decision further. From the previous chapter, one understands that the source extraction part of `ssos` was significantly increased. For `PP`, its SExtractor parameters are much more strict and far less sources are extracted as its goal is not to find faint objects. Having the same parameters would further increase the processing time for little to no results. This is not a real problem when processing fresh data each day, but increasing significantly the processing time for the 15 years of data of TRAPPIST is probably not suited if deemed not useful. Another good reason for separate pipelines is the fact that `PP` is extremely robust and only needs to be ran once on the images, whereas one might want to run `ssos` a second time with different parameters if it looks necessary. Having two pipelines merged with each others would probably impede `ssos` if it needs to be ran twice.

A plot of the processing time of the `automated SSOS pipeline` can be found on Figure 4.2. The processing time is directly linked to the number of images, but it is also dependant on SExtractor: the more sources that are extracted, the more material `ssos` and `PP` need to work on. Moreover, the more objects are retrieved by both pipeline, the more outputs are produced. At most, the pipeline ran for around 3 hours on the main

data computer of the TRAPPIST control room, equipped with an Intel Core i7-7800X @ 3.50 GHz × 12 and 64 Gb of RAM.

4.4 Remaining improvements

To conclude this chapter, we list a number of things that could be addressed if judged necessary. Note that the following modifications would be huge to perform.

First, to have a better synergy between `ssos` and `PP`, and in particular to make use of the discoveries of the former, it is possible to modify pp_distill. The idea would be for it to no longer be ran blindly but instead use the sky coordinates of the extracted objects of `ssos` in order to perform the photometry directly on its retrieved objects. This is accessible through the "positions" argument of the function. With such modification, it would need to be ran for each object and once more for the variable stars. The number of false-positives would have to be low to not spend a large amount of processing time on them.

Second, and probably a more pertinent improvement that could be made, is the use of the remaining functions offered by `PP`. Indeed, the pp_combine and pp_stackedphotometry could be used to performed the so-called *track & stack*. The idea is, by knowing the position of the extracted source on each image, to stack them in order to increase its SNR. This would allow the pipeline to detect fainter objects (see Figure 5.1 in Chapter 5 for our current detection capabilities).

Chapter 5

The `automated SSOS pipeline`, Part 3: results

In this final chapter, we present the results we obtained with the `automated SSOS pipeline`, ranging from the recovery efficiency to the period determinations of the recovered objects.

5.1 Preliminary matter

5.1.1 Data processed

In the following, we present the results we obtained from the data that was processed, which consists of:

1. for TS: the nights starting December 13th, 2019 and ending on March 23rd, 2020. This represents a total of 100 nights while in reality, 86 nights were available. The nights of June 3rd and July 3rd, 2021 were also processed;

2. for TN: the night of September 8th, 2020.

A total of 89 nights were processed. We mostly focused on data from TS starting backwards from the 23rd March 2020 as it was the last night of observation before the observatory was closed due to the COVID-19 pandemic. Because we concatenated the nights, we often have the observation of the same target across several nights and thus the same objects in the images, allowing us to have more material for lightcurves analysis or at least more chances for a recovery. The other nights that were processed serve as a check to the successful operation of the pipeline on more recent data for TS, and on available data for TN.

5.1.2 Lightcurve analysis

From the outputs of the pipeline, it is possible to perform lightcurve analysis if we have sufficient recoveries (measured in data points) and sufficient precision on the magnitude (measured directly from the magnitudes that are retrieved[25]).

[25]It is possible, and common, to have successful recoveries for fainter targets, but the computed magnitudes are not of good quality.

In the following, the periods we compute are for known objects having sufficient recoveries allowing to have at least one full period (one rotation period for asteroids, one cycle of variability for variable stars). The periods were computed using `Peranso` (`Light Curve and Period Analysis Software`)[26], a shareware program. It features various period analysis methods. We used the Fourier Analysis of LightCurves (FALC [44] as it is a standard method for asteroid lightcurve period analysis. As it is suggested by the developers of `Peranso`, this method can be extended to variable star analysis as it is one of the two methods that uses the error bars of the magnitudes during the period computation[27].

5.2 Results

5.2.1 `ssos` recoveries

From the 89 nights that were processed, we report the retrieval of 31 different objects across 53 total detections.

As we previously wrote in Chapter 3, some bright asteroids are not recovered on the first run of the pipeline and a second run is needed with the FILTER_MOTION being deactivated. The faintest asteroid recovered is 2000 WX132 at magnitude 20.5. In fact, this object was retrieved on the night of March 20th and March 23rd, 2020. This is in adequacy with the expected magnitude limit of the TRAPPIST telescopes. Indeed, mag 21 can only be reached with the largest exposure time and without the use of any filter. Such observations occur only with the specific objective of finding new asteroids.

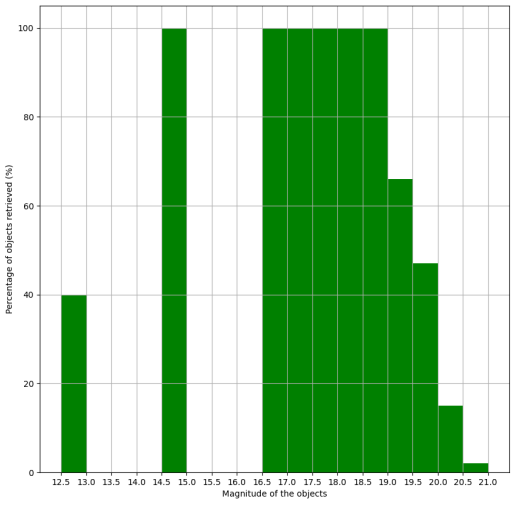

Figure 5.1: Histogram of the percentage of known asteroids that were recovered between magnitude 12.5 and 21. The gaps appear because no asteroids at such magnitudes were in the images. It is possible to reach 100% recovery at magnitude 12.5 by changing the filtering parameters.

[26] `https://www.cbabelgium.com/peranso/`

[27] `https://www.cbabelgium.com/peranso/UserGuideHTML/FALCHarris.html`

Figure 5.1 shows the percentages of known asteroids that are recovered for each interval of 0.5 mag. Comparing with the results obtained by Sicorello last year (see Figure 6.8 p. 50 in his master thesis) we clearly see an improvement in our detections. Indeed, we have 100% recovery up to magnitude 19 (compared to its 75% up to this value). Between magnitude 19 and 19.5, our results are similar. For magnitude 19.5 to 20, we report a slight increase in recoveries. For magnitude 20 to 20.5, we reach 15% recoveries (compared to less than 10% in his work) and we even have 2 detections at magnitude 20.5. We conclude that the new configuration of `ssos` is much better than before, reaching 100% recoveries up to magnitude 19.

Table 5.1 summarises the number of detections for each known asteroid recovered by `ssos`. We give the apparent magnitude for each object and the duration for which the asteroid was detected. We add the filter and exposure time that were used for the detection to give clues to the type of observation we had (asteroids inside the ecliptic or exoplanet transits usually away from it). No new objects were found in the images of the nights that were processed.

Asteroid name	Apparent magnitude	Number of recoveries	Duration of detection (min)	Filter	Exposure time
1994 YC4	19.4	1	150 min	I+z	80 s
1995 SO39	18.9	1	45 min	z	120 s
1997 AF22	17.5	1	250 min	I+z	20 s
1998 QQ93	16.9	2	375 min	I+z	80 s
1998 UO19	18.5	1	200 min	I+z	80 s
1999 JV80	18.0	1	100 min	I+z	50 s
1999 SW10	18.6	1	100 min	I+z	80 s
2000 CS103	18.1	1	250 min	I+z	50 s
2000 LS10	20.0	1	40 min	z	120 s
2000 QM138	19.1	1	100 min	I+z	50 s
2000 WX132	20.5	2	300 min	R	40 s
2001 FS81	18.8	1	100 min	z	120 s
2001 OT98	19.6	2	450 min	I+z	45 s
2001 SU128	18.4	1	70 min	B	120 s
2001 SY156	19.1	2	450 min	I+z	45 s
2002 LP55	19.8	4	1000 min	R	40 s
2002 TJ196	19.0	1	150 min	I+z	50 s
2002 XD58	18.7	1	100 min	I+z	50 s
2005 WM89	19.9	2	250 min	I+z	80 s
2006 HU78	20.0	3	800 min	R	45 s
2006 WM86	19.2	1	250 min	I+z	80 s
2007 CH5	19.5	1	60 min	B	120 s
2008 YD10	19.7	1	200 min	I+z	80 s
(105) Artemis	12.8	4	1400 min	R	30 s
(324) Bamberga	12.7	4	1200 min	R	40 s
(6055) Brunelleschi	18.2	1	150 min	I+z	80 s
(17265) Debennett	18.4	2	200 min	I+z	30 s
(27) Euterpe	10.7	1	50 min	R	30 s
(3395) Jitka	16.5	1	200 min	R	30 s
(208) Lacrimosa	14.6	5	1200 min	R	30 s
(3249) Musashino	17.1	2	550 min	I+z	20 s

Table 5.1: Summary of the detection recoveries performed by `ssos`.

5.2.2 Lightcurve compilation

Hereafter, on Figure 5.2 and 5.3, we display four lightcurves obtained with PP. They belong to the asteroids (105) Artemis, (324) Bamberga, (208) Lacrimosa and (3249) Musashino. The first three were targets of observations, whereas the last was retrieved in the images of SP0900+2150. Four more lightcurves that are less useful can be found in Appendix C.

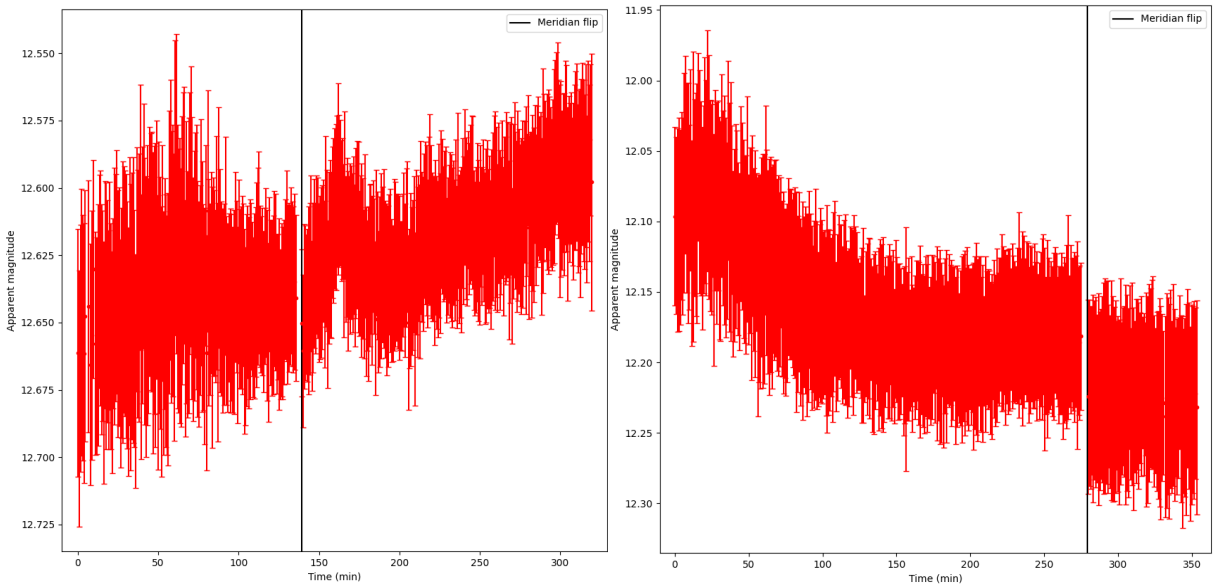

Figure 5.2: Left: lightcurve of the asteroid (105) Artemis, retrieved on the night of January 25th, 2020 (TS). Right: lightcurve of the asteroid (324) Bamberga, retrieved on the night of February 19th, 2020 (TS).

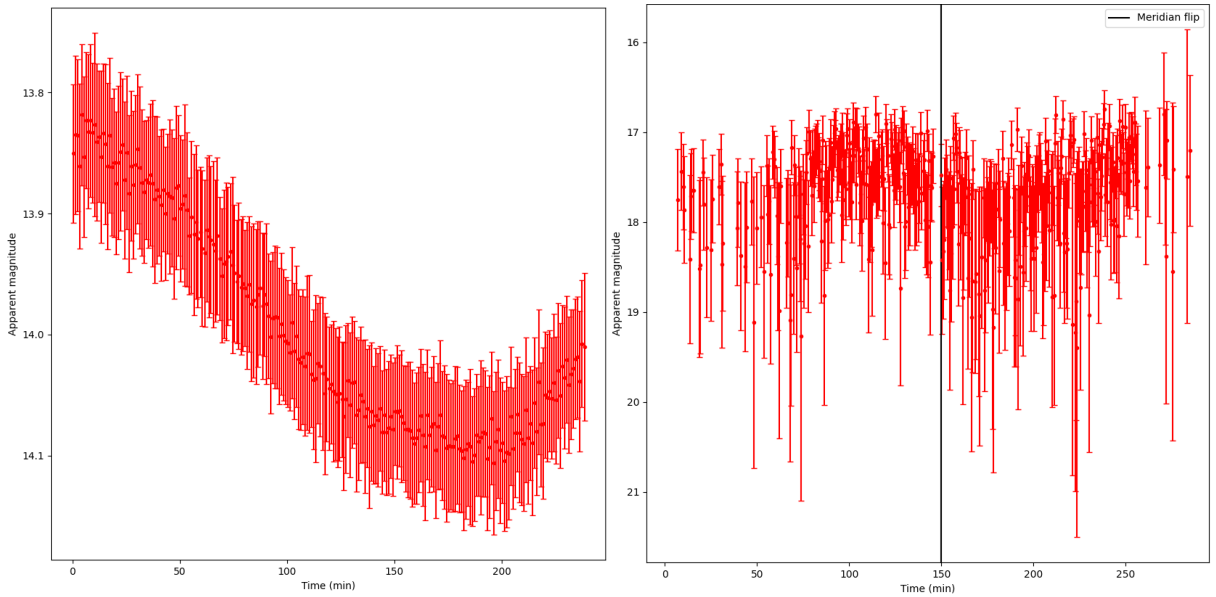

Figure 5.3: Left: lightcurve of the asteroid (208) Lacrimosa, retrieved on the night of February 18th, 2020 (TS). Right: lightcurve of the asteroid (3249) Musashino, retrieved on the night of March 9th, 2020 (TS).

5.2.3 Period determination

We start the discussion by presenting the retrieved asteroids that have a known period. This information can be found on Table 5.2.

Asteroid name	Known period (h)	Computed period (h)
1997 AF22	5.19	X
1999 JV80	1.40239	1.46600
2000 LS10	14.532	X
2001 SY156	6.229	6.244
2002 XD58	2.9649	X
(105) Artemis	37.150	X
(324) Bamberga	29.43	X
(27) Euterpe	10.4082	X
(3395) Jitka	18.293	X
(208) Lacrimosa	14.085	14.084
(3249) Musashino	4.552717	4.582400

Table 5.2: Asteroids that have a known rotation period and that were retrieved by the pipeline. Four periods were computable using `Peranso`. The values of the periods were found on the JPL Small-Body Database Browser (`https://ssd.jpl.nasa.gov/sbdb.cgi`, last consulted on August 16th, 2021).

By comparing this table with the duration of the detection of each asteroid that were retrieved by the pipeline (see Table 5.1), we can forget about all asteroids but 4. Indeed, we have a minimum of about 10% of a lightcurve for 2000 LS10, and at most 80% of a lightcurve for 1997 AF22. Plus, for some asteroids, for example (324) Bamberga, we may have 60% of its lightcurve just by considering the time of observation, whereas in practice we have repeated parts of it. Therefore, the only 4 asteroids for which we have a longer time of observation compared to their period of rotation are: 1999 JV10, 2001 SY156, (208) Lacrimosa and (3249) Musashino. Even though `Peranso` found a good value of the rotation period of 1999 JV10 ($P = 1.46600$ h), our only lightcurve is not of good quality. We have two lightcurves for 2001 SY186, but one of them is bad and thus computing its phased lightcurve was irrelevant. This is a frequent problem when dealing with asteroids that are barely visible in the images. However, for the remaining two asteroids, we have both enough data and sufficiently good lightcurves to retrieve their periods and obtain their phased lightcurves. The phased lightcurves of (208) Lacrimosa and (3249) Musashino can be found on Figure 5.4 and 5.5 respectively.

It is clear that the phased lightcurve of (208) Lacrimosa is missing a piece. This is due to its rotation period of 14.085 h, which is close to exactly half a day. This means that between two nights, the lightcurve is not shifted by much and we can observe the same part over consecutive nights. We did not use all the data that was available as the phased lightcurve was looking worse, and as a consequence, we are missing a quarter of the phased lightcurve.

For (3249) Musashino, as the object had an apparent magnitude of 17.1, its phased lightcurve is noisier, but its general shape is visible.

No rotation periods could be computed for the other asteroids as we have either too little data or data of insufficient quality for faint objects (see Appendix C, which is part of the reason for which their rotation period is unknown.

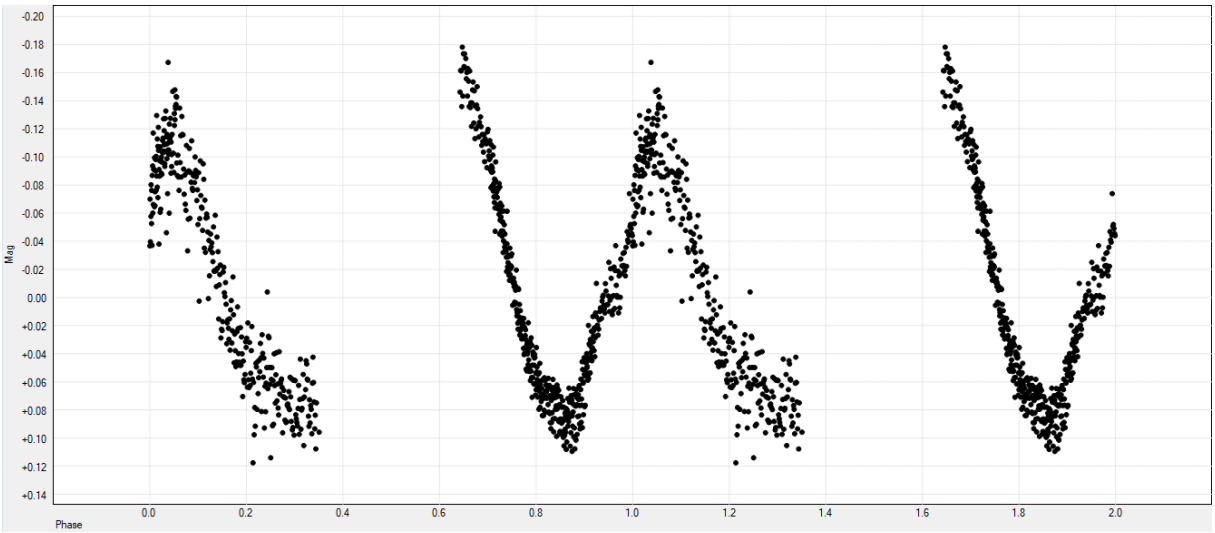

Figure 5.4: Phased lightcurve of the asteroid (208) Lacrimosa, obtained with `Peranso`.

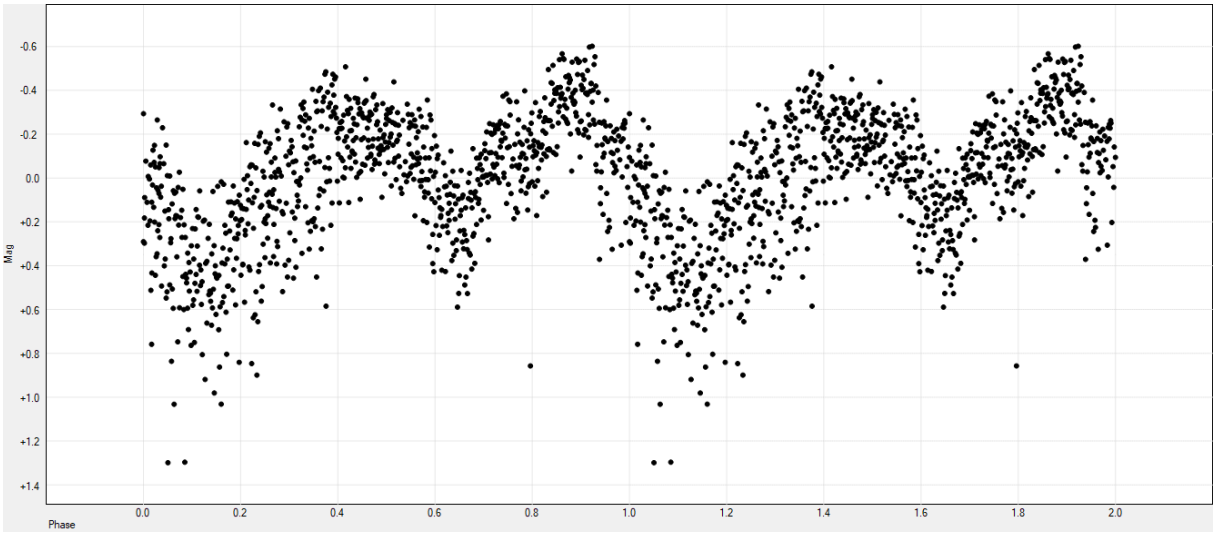

Figure 5.5: Phased lightcurve of the asteroid (3249) Musashino, obtained with `Peranso`.

5.2.4 Limiting magnitudes

As a final result, we present a summary of our knowledge on the limiting magnitudes of the TRAPPIST telescopes. We have shown that retrieving asteroids fainter than mag 20.5 is impossible during a standard observation. In practice, for each observing conditions that can be chosen by the TRAPPIST team, the limiting magnitude depends on the filter and the exposure time. This is why we can recover asteroids of magnitude 20 but only under certain conditions. In Table 5.3, we give the magnitude of the faintest asteroid that was recovered for each set of filter / exposure time that we processed. This can give clues of the results we should expect of the pipeline. However, this is not a definitive proof of its capabilities as we can have exterior factors that allow an easier or harder recovery, like varying weather conditions or Moon illumination. Moreover, surprising discrepancies between two similar observing conditions (for example the weaker recovery in the R filter with a binning 2 compared to the same configuration but with a binning 1) can be explained by the absence of fainter asteroids in the field that could have otherwise been recovered.

Filter	Binning	Exposure time (s)	Magnitude limit
B	1	125	20
V	1	120	20
R	1	30	17
		40	20.5
		45	20.5
	2	30	15
		50	15
I+z	1	20	18.5
		30	18.5
		45	20
		50	19.5
		80	20
z	1	120	20.5

Table 5.3: Table summarising the limiting magnitudes of the TRAPPIST telescopes. This result was obtained with the data that was extracted from a sample of 89 nights. For 13 different observing strategies, we have thus only a few reiteration and the results can evolve. The limiting magnitude is rounded up to the nearest half-integer.

5.2.5 Variable stars recoveries

As our work was mainly on small Solar System objects and because variable stars are only an added value to the pipeline, the results relative to this topic is not discussed in the main body but can be found in Appendix A.

Conclusion

The two TRAPPIST telescopes of the University of Liège operates almost every night throughout the year. Today, their combined database account for around 15 years of data. With observing time spreads evenly on the direct observation of small Solar System objects and the characterisation of exoplanet transits, the TRAPPIST telescopes offer data that: (1) is rich in known objects and (2) has potential for detections of unknown objects.

During the academic year 2020-2021, Sicorello started working on the `automated SSOS pipeline`, a tool specially designed for the TRAPPIST telescopes in order to search for small Solar System bodies in the archives. Based on the `ssos Pipeline`, it had already proven its capabilities during his work.

As it was discussed in Chapter 3, the filtering performed by the `ssos Pipeline` has been refined, and the pipeline itself was significantly improved.

In Chapter 4, we discussed the missing pieces that were available to further improve our scientific outputs. Using the `Photometry Pipeline`, the addition of differential photometry allowed us to obtain rotation lightcurves of some asteroids. Furthermore, the pipeline reliably extract the variable stars that are present in the images, supplementing a new added value at almost no cost.

The results we presented in Chapter 5 are a proof of the upgrades that were made to the `automated SSOS pipeline`. Recovering asteroids up to magnitude 19 with a 100% success rate is, by itself, extremely encouraging. The retrieval of an asteroid at magnitude 20.5, twice, is a first step in the discovery of new objects in the archives. The lightcurves we obtained generally do not allow us to find the asteroid rotation period, but they can nonetheless provide useful estimation and more data to lightcurve databases. Processing many more nights could extend our own database, allowing us to compute more periods.

More milestones are yet to be passed, and there is still room for the pipeline to evolve.

First, the pipeline can be finalised in order to be ran on the fresh data that is produced by the TRAPPIST telescopes every night, providing direct outputs for all the future data.

Second, a better merger between the two pipelines, `ssos` and `PP`, could provide similar improvements than those that were made in this work. Indeed, with hindsight, we could expect the outputs of the `Photometry Pipeline` to be refined as we did to those of the `ssos Pipeline`, yielding even better results.

Third, the pipeline could be adapted to run on the Search for habitable Planets EClipsing ULtra-cOOl Stars (SPECULOOS) telescopes. With larger mirrors and narrower field of views compared to the TRAPPIST telescopes, combined with long exposures when observing ultra-cool stars away from the ecliptic, the SPECULOOS telescopes could provide information on lesser known asteroids, or have a better chance of making new discoveries.

Lastly, track and stack options are still available to the `automated SSOS pipeline`. Such an addition would most certainly take a lot of work to be added flawlessly to the current simple process of the pipeline.

With 53 detections of 31 different asteroids and 99 detections of 51 different variable stars across 89 nights, the pipeline has shown the heights that could be reached. With 15 years of data for the TRAPPIST telescopes, the amount of information that can be extracted is huge. We have hopefully shown that new discoveries are within reach.

Appendix A

Variable stars recovered by PP

For completeness, we present the results about variable stars relative to the PP part of the pipeline. From the 89 nights that were processed, we report the retrieval of 51 variable stars. We split the results between the various catalogues they belong to. We give only a short description of each survey and list our recoveries. The period of a short variable star we retrieved was computed, and our lightcurves can be sent to the respective database of each star.

A.1 Two Micron All-Sky Survey stars

The Two Micron All-Sky Survey (2MASS)[28] was a near-infrared survey of the entire sky performed by the University of Massachusets and the Infrared Processing and Analysis Center (IPAC) between 1997 and 2001. Observations were made with two 1.3 m telescopes located in Mount Hopkins, Arizona, and Cerro Tololo, Chile [45].

We report the retrieval of 4 stars named after this survey, their respective number of recoveries is summarised in Table A.1.

Star name	Number of recoveries
2MASS J09312228-1717425	4
2MASS J10424135-2416050	4
2MASS J11024596-1624222	17
2MASS J12235208-0858432	2

Table A.1: Names and number of recoveries of the 4 2MASS stars that were retrieved.

A.2 All Sky Automated Survey stars

The All Sky Automated Survey (ASAS)[29] is a Polish project supported by the State Committee for Scientific Research (KBN) that started in 1997. It consists of a pair of telescope,

[28] https://irsa.ipac.caltech.edu/data/2MASS/docs/

[29] http://www.astrouw.edu.pl/asas/?page=main

ASAS-South in Las Campanas Observatory, Chile, and ASAS-North in Haleakala, Maui. Its objective is to catalogue variable stars through a constant photometric monitoring of around 10 million stars brighter than magnitude 14 [46].

We report the retrieval of a single star named after this survey, which was recovered only once (see Table A.2).

Star name	Number of recoveries
ASAS J085349-2509.1	1

Table A.2: Name of the single ASAS star that was retrieved.

A.3 All Sky Automated Survey for SuperNovae stars

Despite its name, the All Sky Automated Survey for SuperNovae (ASAS-SN)[30] is not linked to the ASAS project. It consists of 24 telescopes spread across Africa, America, Asia and Europe. They allow a complete survey of the sky in search for transient events such a supernovae [47].

We report the retrieval of 16 stars named after this survey, their respective number of recoveries is summarised in Table A.3.

Star name	Number of recoveries
ASASSN-V J061107.91-334600.2	7
ASASSN-V J073605.51-734123.0	2
ASASSN-V J093148.13-171358.0	4
ASASSN-V J161825.66-224024.5	1
ASASSN-V J122407.25-105215.7	1
ASASSN-V J124719.25-561132.9	1
ASASSN-V J124751.97-564153.2	1
ASASSN-V J124805.09-564051.5	1
ASASSN-V J124809.33-564135.5	1
ASASSN-V J124813.59-564113.1	1
ASASSN-V J125110.45-582459.8	1
ASASSN-V J125118.85-584848.0	1
ASASSN-V J125137.76-592042.8	1
ASASSN-V J125138.53-584833.2	1
ASASSN-V J125214.19-592148.7	1
ASASSN-V J125254.13-592124.3	1

Table A.3: Names and number of recoveries of the 16 ASAS-SN stars that were retrieved.

[30] `http://www.astronomy.ohio-state.edu/~assassin/index.shtml`

A.4 Catalina Sky Survey and Siding Spring Survey stars

The Catalina Sky Survey (CSS)[31] is a project funded by NASA, that consists of three telescopes located in the Santa Catalina Mountains, Arizona. The project started in 1998 with the objective of finding NEOs and especially PHAs. It is now the most prolific NEOs survey with the discovery by itself of close to half of the population.

The Siding Spring Survey (SSS) was the Southern-hemisphere counterpart of the CSS. Operated by the University of Arizona and the Australian National University, the survey started in 2004 and ended in 2013. The Siding Spring Observatory is located in Siding Spring, Australia.

Although variable stars are not their main objective, their data contains a multitude (up to 5.4 million) variable candidates [48].

We report the retrieval of 8 stars named after these surveys, their respective number of recoveries is summarised in Table A.4.

Star name	Number of recoveries
CSS J085953.9+214928	2
SSS J085348.1-245930	2
SSS J104311.7-443256	1
SSS J121831.9-423704	1
SSS J134632.3-314248	3
SSS J161835.7-224237	1
SSS J161944.0-224610	1
SSS J162129.5-224723	1

Table A.4: Names and number of recoveries of the single CSS star and 7 SSS stars that were retrieved.

A.5 Ecliptic Plane Input Catalog stars

The Ecliptic Plane Input Catalog (EPIC) database was produced during the K2 mission of the Kepler[32] spacecraft of NASA, launched in 2009. It was initially supposed to monitor thousands of stars for transiting exoplanets. The loss of two out of its four reaction wheels put an end to this mission in 2013. In 2014, a new assignment was given to the spacecraft: the monitoring of stars inside the ecliptic plane. The motivation behind this decision was to make use of its photometric precision without being impede by the loss of the reaction wheels. Indeed, having the spacecraft parallel to the ecliptic plane reduces the torque exerted by the solar wind, and allows it to be operated with only its remaining reaction wheels and fuel. Its mission ended in 2018, and EPIC results are available on the Mikulski Archive for Space Telescopes (MAST)[33] with references [49].

[31] `https://catalina.lpl.arizona.edu/`

[32] `https://www.nasa.gov/mission_pages/kepler/overview/index.html`

[33] `https://archive.stsci.edu/`

We report the retrieval of 10 stars named after this survey, their respective number of recoveries is summarised in Table A.5.

Star name	Number of recoveries
EPIC 204242600	1
EPIC 204256494	1
EPIC 204279000	2
EPIC 204287798	2
EPIC 204290918	1
EPIC 204296346	2
EPIC 204298932	1
EPIC 204302376	1
EPIC 204315760	2
EPIC 204321959	2

Table A.5: Names and number of recoveries of the 10 EPIC stars that were retrieved.

A.6 Gaia stars

Gaia[34] is an ESA spacecraft, launched in 2013, whose mission is to provide astrometric measurements of more than 1% of the stars of our galaxy in order to provide its most precise 3D map [50]. In 2021, the Early Data Release 3 (EDR3) was made available [51]. It offers a significant improvement over the previous release, which was already one of the better star catalogues.

We report the retrieval of 1 star named after this survey, which was recovered only once (see Table A.6).

Star name	Number of recoveries
Gaia16cem	1

Table A.6: Name of the single Gaia star that was retrieved.

A.7 General Catalogue of Variable Stars and New catalogue of Suspected Variable stars

The General Catalogue of Variable Stars (GCVS)[35] and the New catalogue of Suspected Variable (NSV) are available from the Lomonosov Moscow State University and Institute of Astronomy of the Russian Academy of Sciences. Researches started in 1948 and the GCVS is currently at its version 5.1 [52].

[34] `https://sci.esa.int/web/gaia/home`
[35] `http://www.sai.msu.su/gcvs/index.htm`

We report the retrieval of 3 stars named after these surveys, their respective number of recoveries is summarised in Table A.7.

Star name	Number of recoveries
DK Mus	1
V0489 Mon	1
NSV 7604	1

Table A.7: Name and number of recoveries of the 2 GCVS stars and the single NSV star that were retrieved.

A.8 Pan-STARRS1 stars

The Panoramic Survey Telescope and Rapid Response System (Pan-STARRS)[36] is a pair of telescope located at the Haleakala Observatory, Maui. Pan-STARRS1 started its operation in 2010. It is a 1.8 m Ritchey–Chrétien telescope equipped with a camera of 1.4 gigapixel (to be compared to the 4.2 megapixels of TS). Similarly to the CSS, PS1 is currently mainly used for the search of NEOs [53].

We report the retrieval of 1 star named after this survey, which was recovered twice (see Table A.8).

Star name	Number of recoveries
PS1-3PI J162037.06-224653.2	2

Table A.8: Name and number of recoveries of the single PS1 star that was retrieved.

A.9 Wide-field Infrared Survey Explorer stars

The Wide-field Infrared Survey Explorer (WISE)[37] is a NASA spacecraft that was launched in 2009. For two years, it scanned the entire sky twice before being put to sleep. It was reactivated in 2013, under the new name of NEOWISE and is now looking for NEOs. Throughout its operation, numerous variable stars are catalogued [54].

We report the retrieval of 2 stars named after this survey, their respective number of recoveries is summarised in Table A.9.

A.10 Zwicky Transient Facility stars

The Zwicky Transient Facility (ZTF)[38] is a survey performed by the Samuel Oschin Telescope at the Palomar Observatory, California. It started in 2017, with the superseding

[36] `https://panstarrs.ifa.hawaii.edu/pswww/?page_id=154`
[37] `https://www.nasa.gov/mission_pages/WISE/mission/index.html`
[38] `https://www.ztf.caltech.edu/`

Star name	Number of recoveries
WISE J064739.8-093918	1
WISE J125420.7-611600	1

Table A.9: Names and number of recoveries of the 2 WISE stars that were retrieved.

Star name	Number of recoveries
ZTF J055748.35+171339.2	6
ZTF J063907.98-084214.9	1
ZTF J064251.55-091047.0	1
ZTF J064326.06-090645.4	1
ZTF J075103.10+233209.3	1

Table A.10: Names and number of recoveries of the 5 ZTF stars that were retrieved.

of the Palomar Transient Factory (PTF). The newly equipped telescope has 16 CCDs of 6144×6160 pixels each, allowing for a broad field of view of 47 square degree. The telescope is able to image the entire northern sky up to mag 20.5 and detect a multitude of variable stars [55].

We report the retrieval of 5 stars named after this survey, their respective number of recoveries is summarised in Table A.10.

A.11 Period determination and phased lightcurves

Most of the variable stars we retrieved are period that are too long to be computed. We present hereafter 4 lightcurves of 4 variables stars from 4 different catalogues.

The last one, ASASSN-V J061107.91-334600.2, has a period of only 0.062 752 d[39]. With 7 recoveries, we can easily compute a period and a phased lightcurve with `Peranso`. We found a value the period of 0.062 758 d and the phased lightcurve can be found on Figure A.3.

[39] `https://asas-sn.osu.edu/variables/317f9ccc-cc10-54de-9c48-a730c46b58ed`

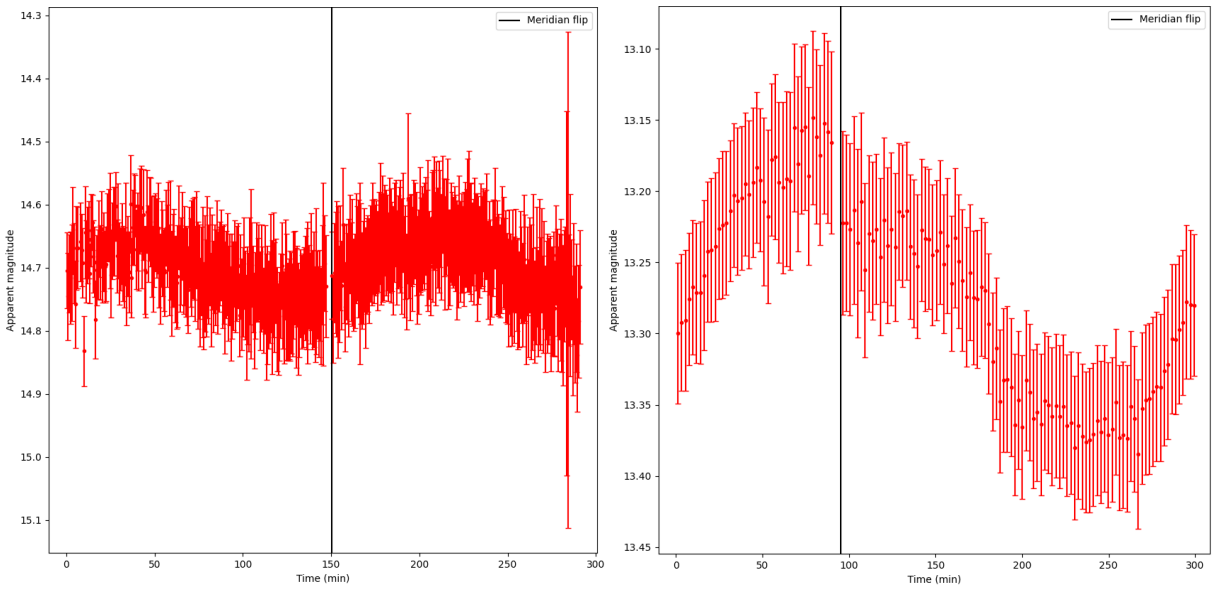

Figure A.1: Left: lightcurve of the variable star CSS J085953.9+214928. Right: lightcurve of the variable star SSS J104311.7-443256.

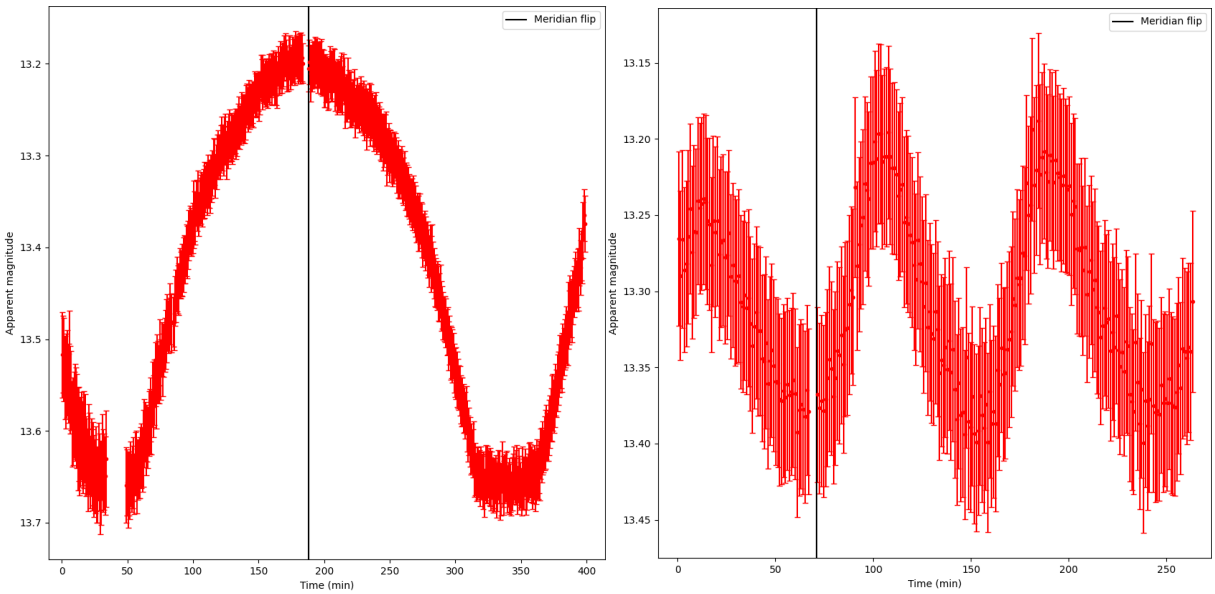

Figure A.2: Left: lightcurve of the variable star WISE J064739.8-093918. Right: lightcurve of the variable star ASSN-V J061107.91-334600.2.

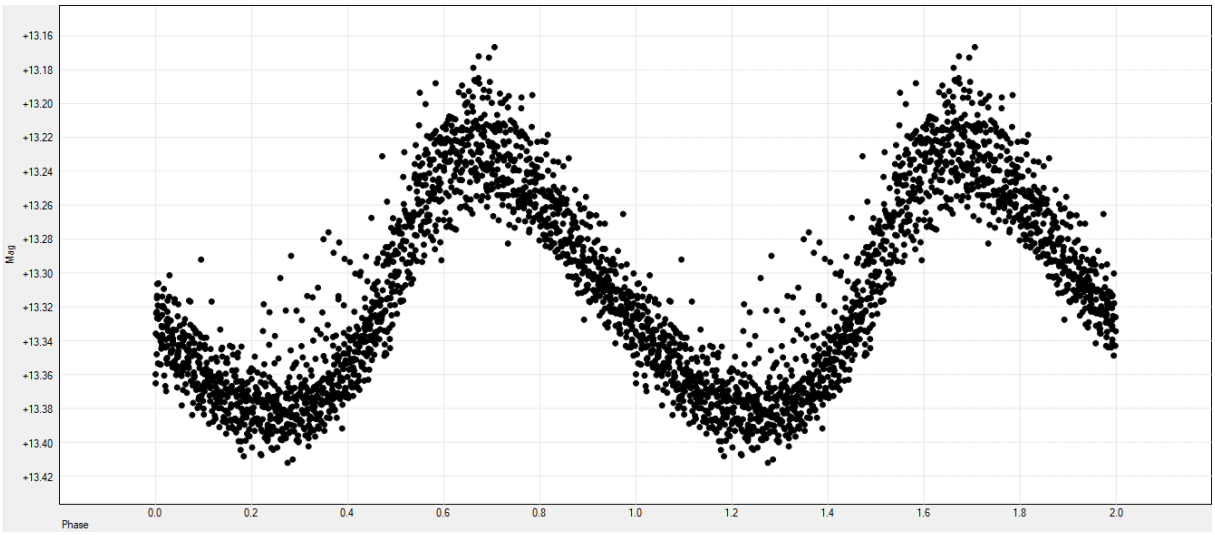

Figure A.3: Phased lightcurve of the variable star ASASSN-V J061107.91-334600.2, obtained with `Peranso`.

Appendix B

PDF summary example

In the following pages, we give the example of a typical PDF report that is produced by the `automated SSOS pipeline`. Here, we take the example of the first field of the night of March 9th, 2020. The target was the star SP0900+2150 and we recovered 3 asteroids between mag 17.0 and 18.5: (17265) Debennett, (3249) Musashino and 1997 AF22. Both Musashino and 1997 AF22 have workable lightcurves as they are bright enough for the observing conditions (20 s of exposure time with a I+z filter). The star CSS J085953.9+214928 was present in the field and recovered by `PP`. Note that the lightcurves of `PP` are not always clearly readable: the pipeline is supposed to automatically remove improper magnitudes which is not perfectly reliable.

For this first field, we have 10 pages. The full PDF of this night contains 25 pages.

TS_20200309

General information on the observation:
Telescope: TS
Date of first image: 2020-03-10T00:04:35.679
Date of last image: 2020-03-10T04:49:46.820
Airmass [start;end]: [2.13;2.06]
Target name: sp0900+2150
Target RA: 09 00 24.00
Target DEC: +21 50 05.0
Nuber of images: 551
Filter: I+z
Binning: 1
Exposure time: 20.0 s
Output folder: /home/ferrais/SSOS/TS_8918_8919_B1R21_sp0900+2150

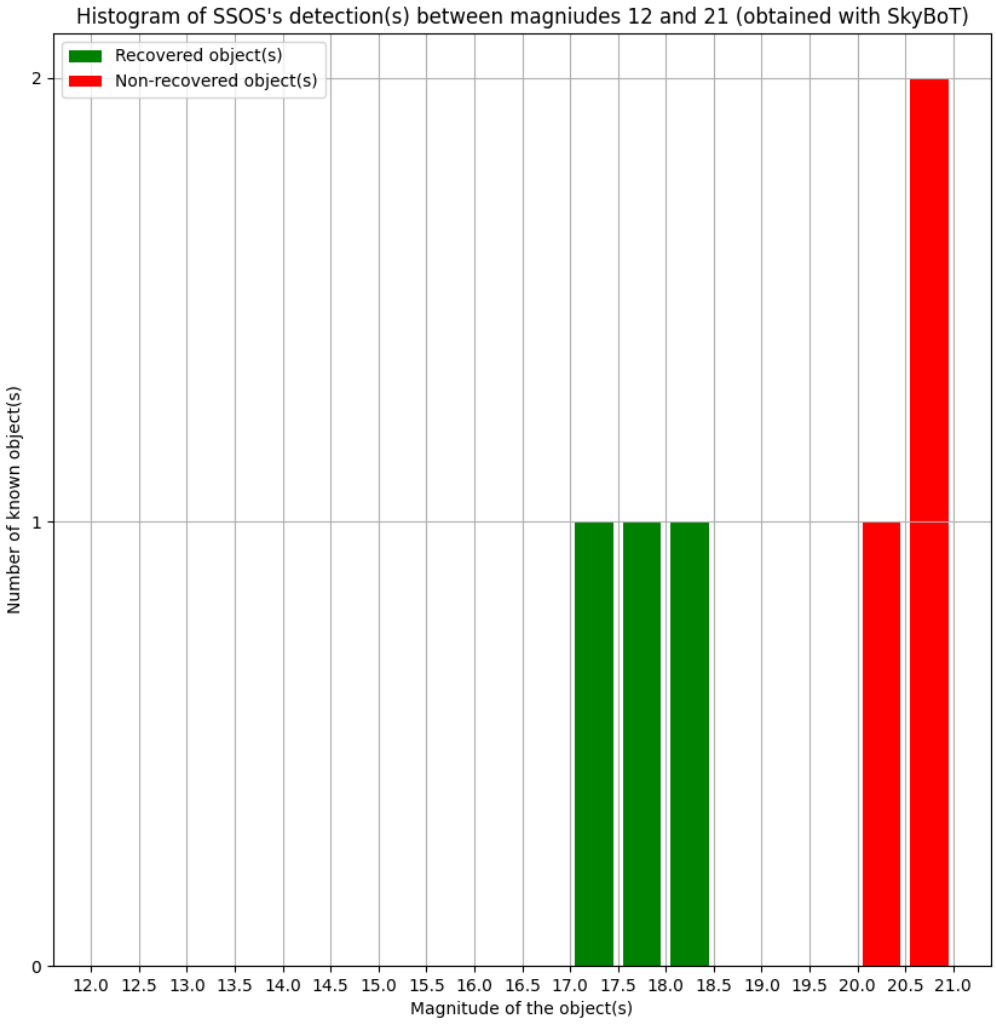

TS_20200309

General information on the observation:
Telescope: TS
Date of first image: 2020-03-10T00:04:35.679
Date of last image: 2020-03-10T04:49:46.820
Airmass [start;end]: [2.13;2.06]
Target name: sp0900+2150
Target RA: 09 00 24.00
Target DEC: +21 50 05.0
Nuber of images: 551
Filter: I+z
Binning: 1
Exposure time: 20.0 s
Output folder: /home/ferrais/SSOS/TS_8918_8919_B1R21_sp0900+2150

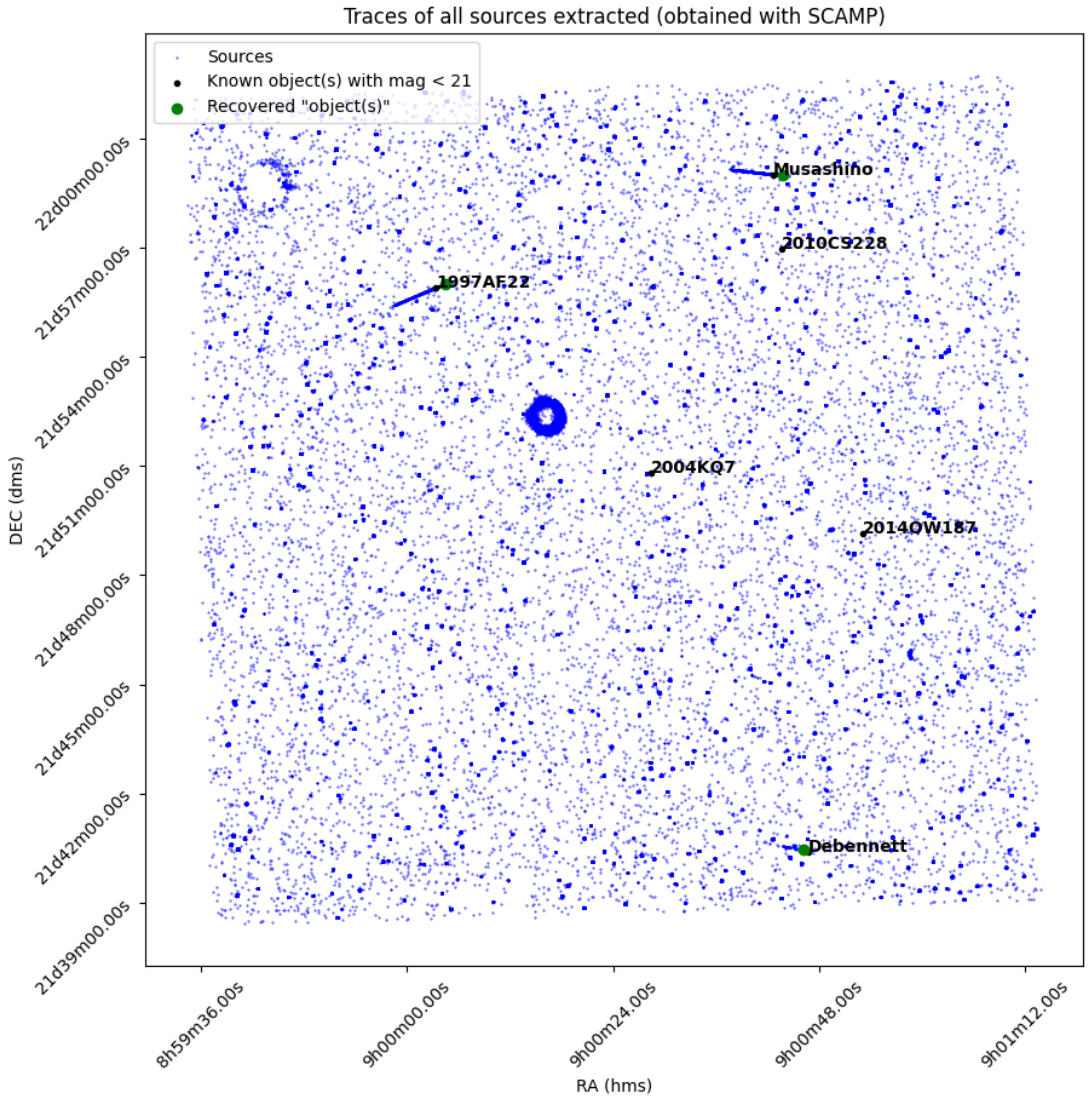

TS_20200309

General information on the observation:
Telescope: TS
Date of first image: 2020-03-10T00:04:35.679
Date of last image: 2020-03-10T04:49:46.820
Airmass [start;end]: [2.13;2.06]
Target name: sp0900+2150
Target RA: 09 00 24.00
Target DEC: +21 50 05.0
Nuber of images: 551
Filter: I+z
Binning: 1
Exposure time: 20.0 s
Output folder: /home/ferrais/SSOS/TS_8918_8919_B1R21_sp0900+2150

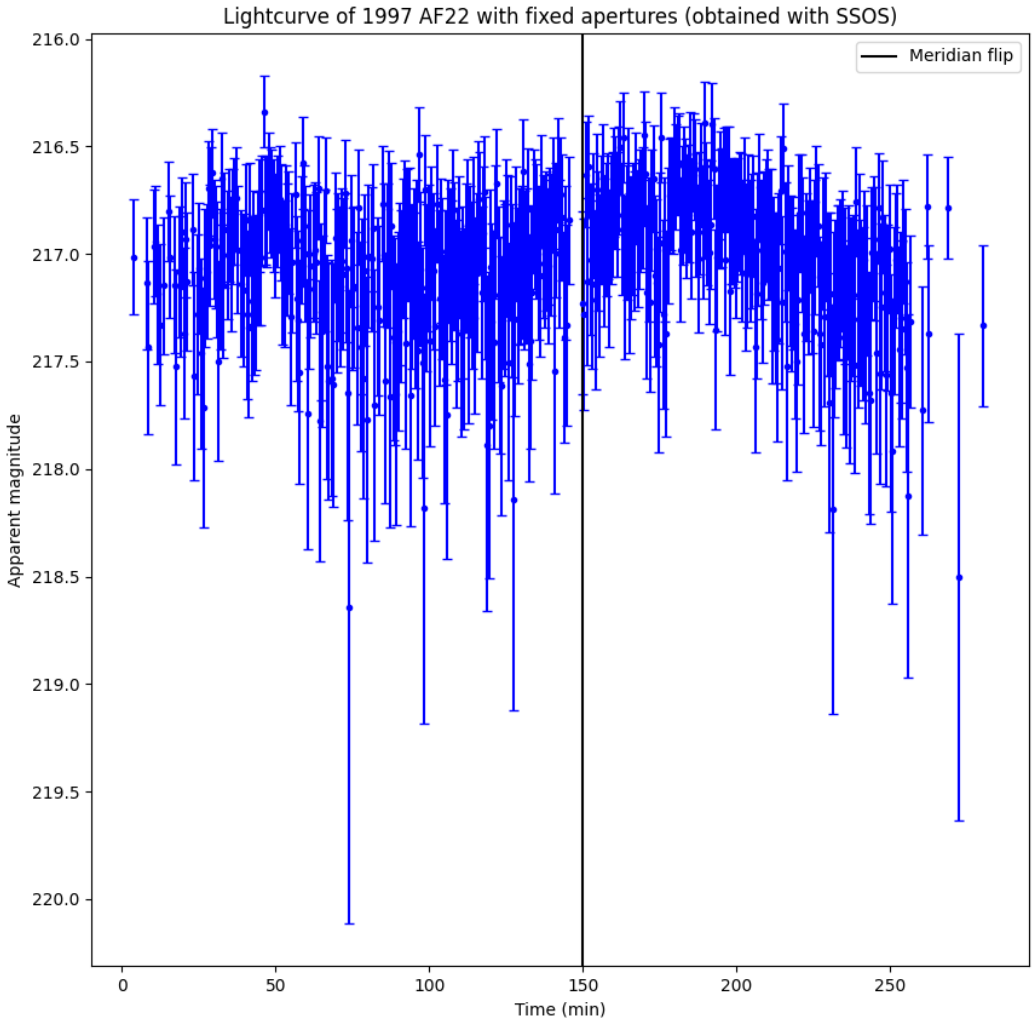

TS_20200309

General information on the observation:
Telescope: TS
Date of first image: 2020-03-10T00:04:35.679
Date of last image: 2020-03-10T04:49:46.820
Airmass [start;end]: [2.13;2.06]
Target name: sp0900+2150
Target RA: 09 00 24.00
Target DEC: +21 50 05.0
Nuber of images: 551
Filter: I+z
Binning: 1
Exposure time: 20.0 s
Output folder: /home/ferrais/SSOS/TS_8918_8919_B1R21_sp0900+2150

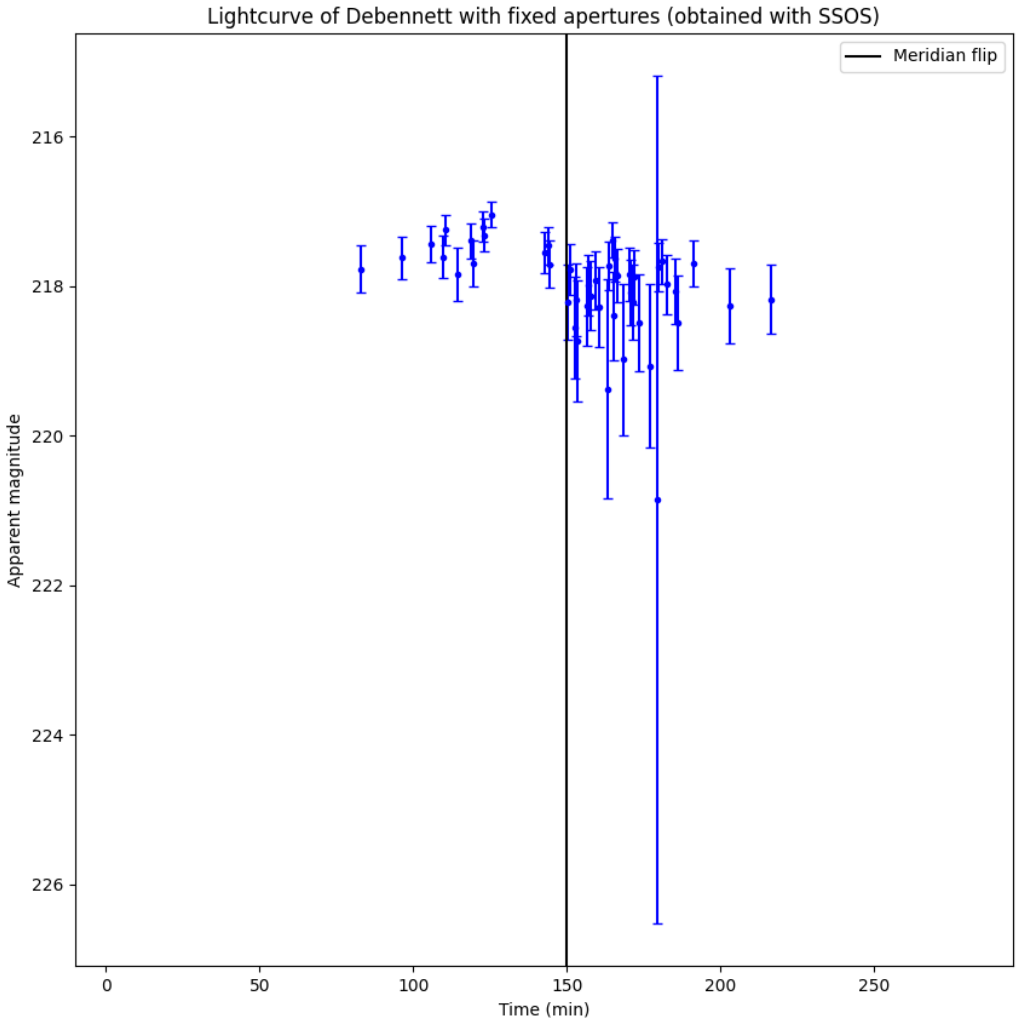

TS_20200309

General information on the observation:
Telescope: TS
Date of first image: 2020-03-10T00:04:35.679
Date of last image: 2020-03-10T04:49:46.820
Airmass [start;end]: [2.13;2.06]
Target name: sp0900+2150
Target RA: 09 00 24.00
Target DEC: +21 50 05.0
Nuber of images: 551
Filter: I+z
Binning: 1
Exposure time: 20.0 s
Output folder: /home/ferrais/SSOS/TS_8918_8919_B1R21_sp0900+2150

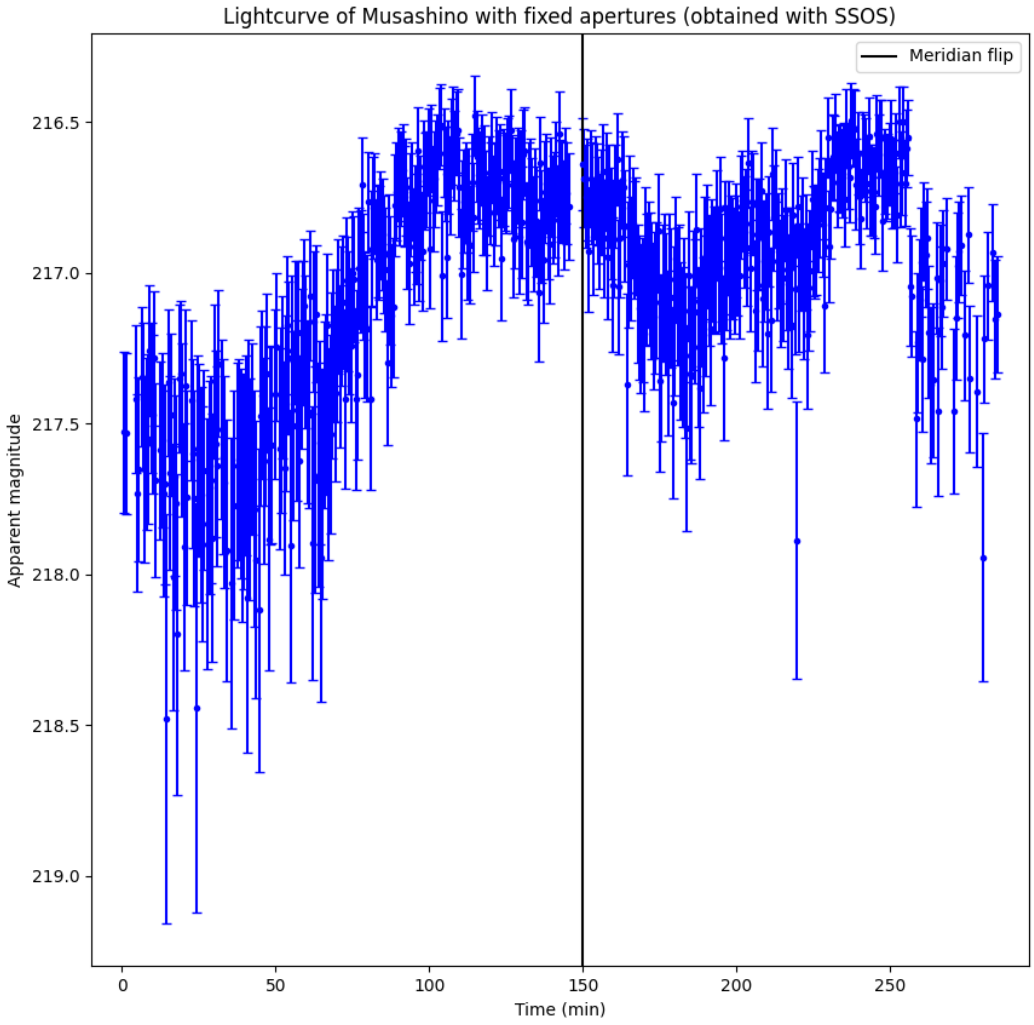

TS_20200309

General information on the observation:
Telescope: TS
Date of first image: 2020-03-10T00:04:35.679
Date of last image: 2020-03-10T04:49:46.820
Airmass [start;end]: [2.13;2.06]
Target name: sp0900+2150
Target RA: 09 00 24.00
Target DEC: +21 50 05.0
Nuber of images: 551
Filter: I+z
Binning: 1
Exposure time: 20.0 s
Output folder: /home/ferrais/SSOS/TS_8918_8919_B1R21_sp0900+2150

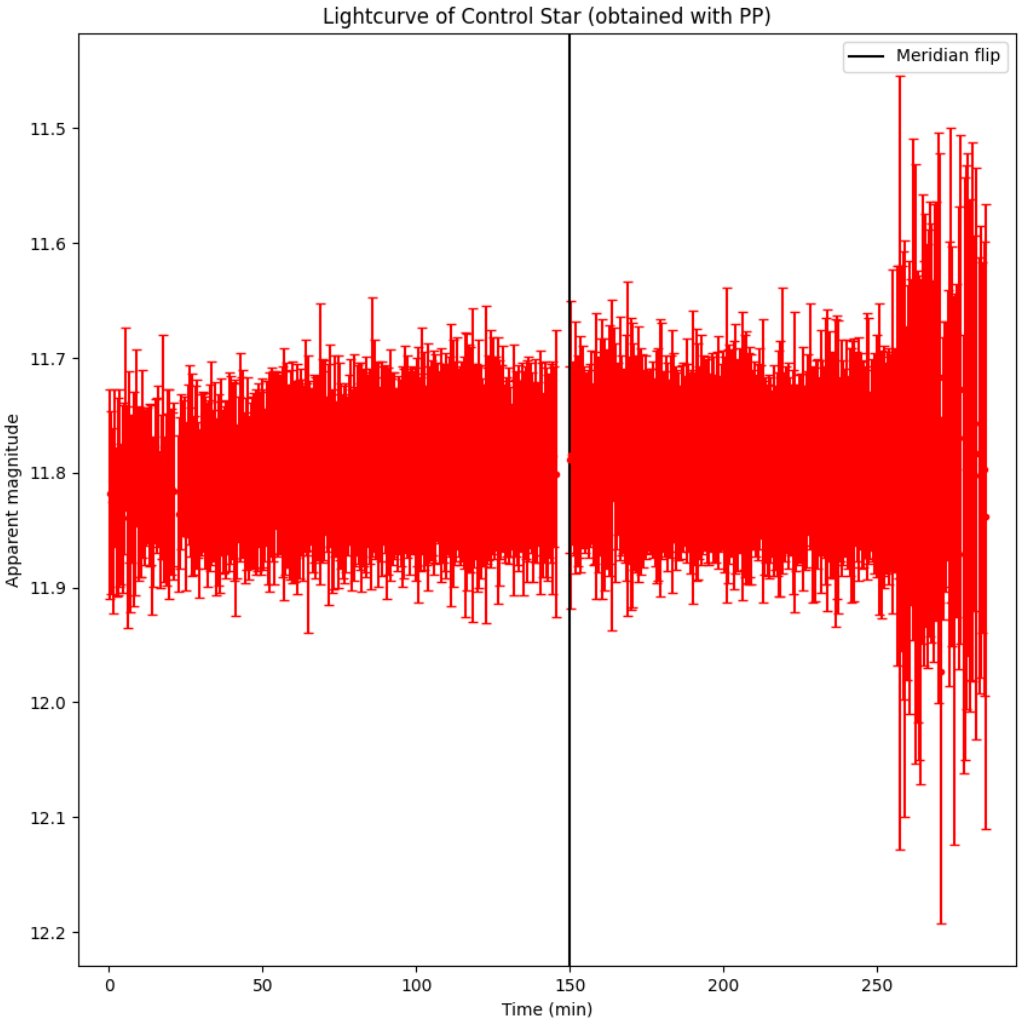

TS_20200309

General information on the observation:
Telescope: TS
Date of first image: 2020-03-10T00:04:35.679
Date of last image: 2020-03-10T04:49:46.820
Airmass [start;end]: [2.13;2.06]
Target name: sp0900+2150
Target RA: 09 00 24.00
Target DEC: +21 50 05.0
Nuber of images: 551
Filter: I+z
Binning: 1
Exposure time: 20.0 s
Output folder: /home/ferrais/SSOS/TS_8918_8919_B1R21_sp0900+2150

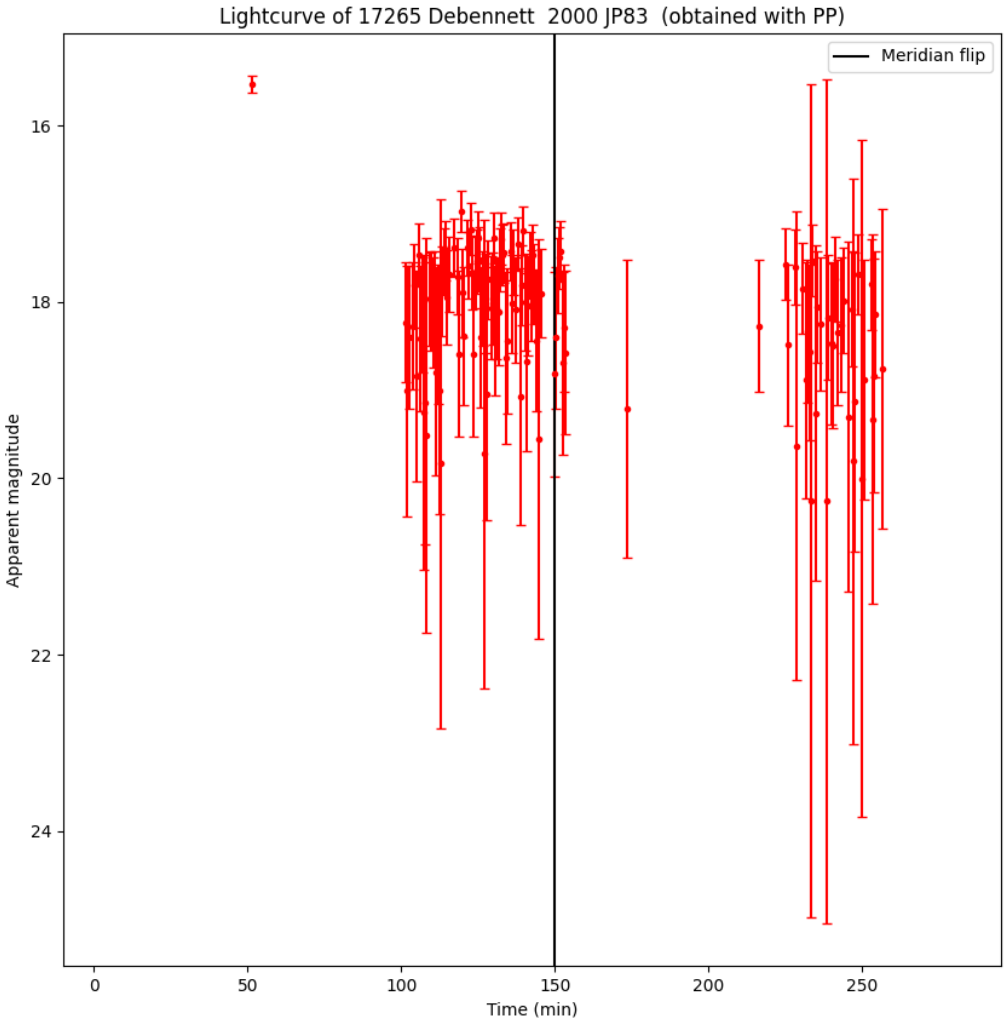

TS_20200309

General information on the observation:
Telescope: TS
Date of first image: 2020-03-10T00:04:35.679
Date of last image: 2020-03-10T04:49:46.820
Airmass [start;end]: [2.13;2.06]
Target name: sp0900+2150
Target RA: 09 00 24.00
Target DEC: +21 50 05.0
Nuber of images: 551
Filter: I+z
Binning: 1
Exposure time: 20.0 s
Output folder: /home/ferrais/SSOS/TS_8918_8919_B1R21_sp0900+2150

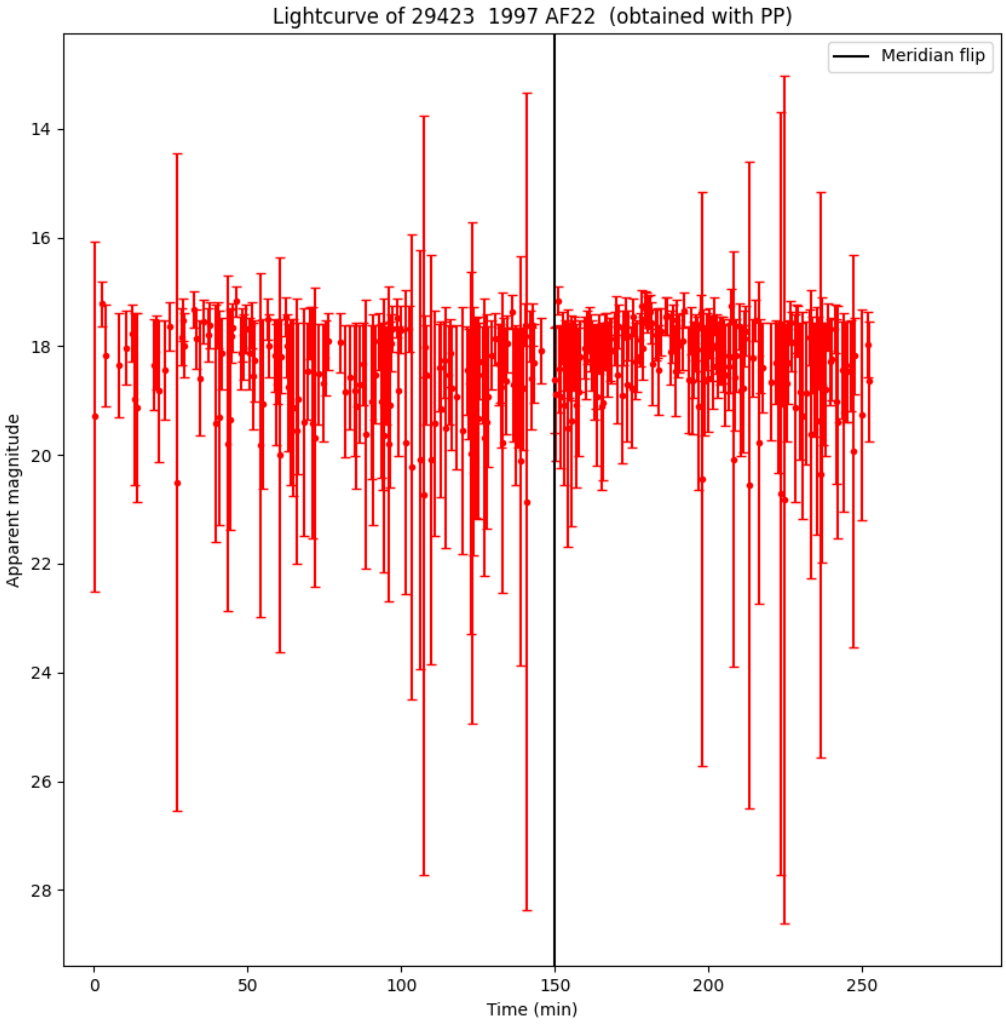

TS_20200309

General information on the observation:
Telescope: TS
Date of first image: 2020-03-10T00:04:35.679
Date of last image: 2020-03-10T04:49:46.820
Airmass [start;end]: [2.13;2.06]
Target name: sp0900+2150
Target RA: 09 00 24.00
Target DEC: +21 50 05.0
Nuber of images: 551
Filter: I+z
Binning: 1
Exposure time: 20.0 s
Output folder: /home/ferrais/SSOS/TS_8918_8919_B1R21_sp0900+2150

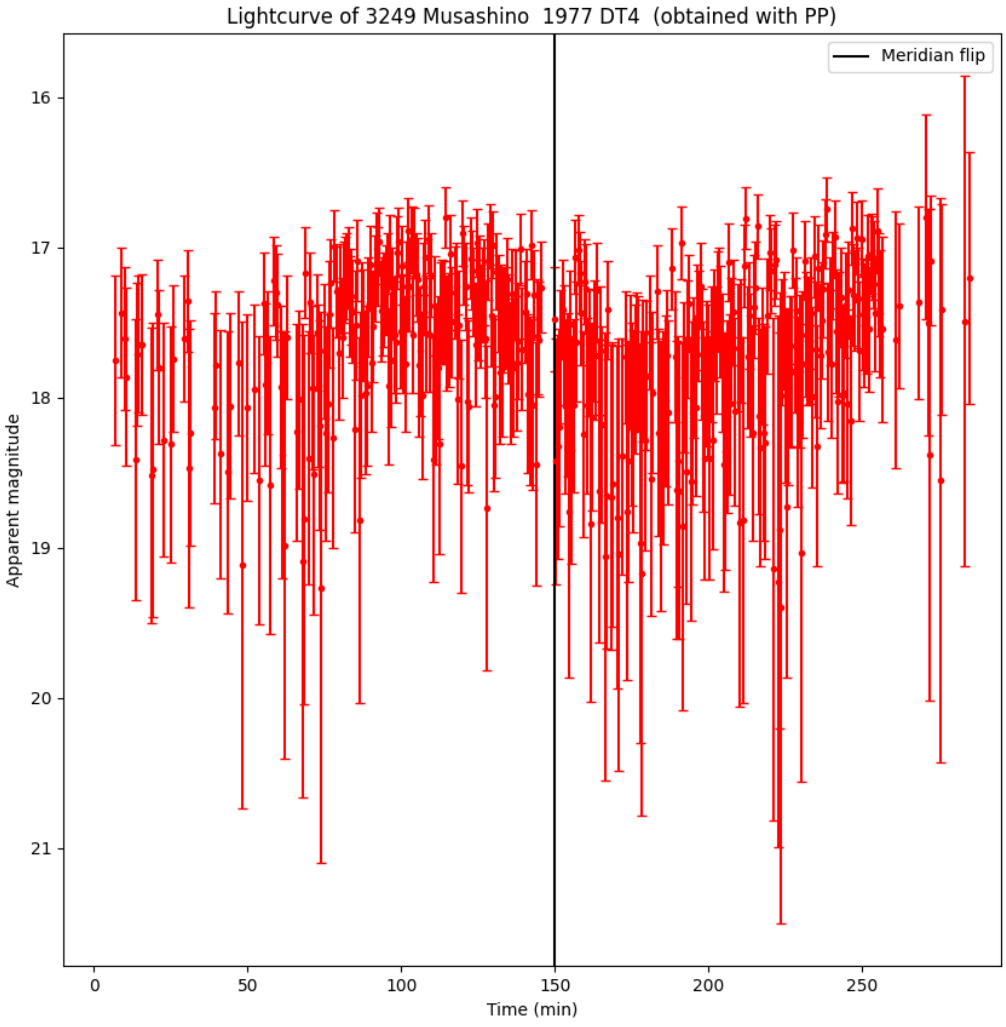

TS_20200309

General information on the observation:
Telescope: TS
Date of first image: 2020-03-10T00:04:35.679
Date of last image: 2020-03-10T04:49:46.820
Airmass [start;end]: [2.13;2.06]
Target name: sp0900+2150
Target RA: 09 00 24.00
Target DEC: +21 50 05.0
Nuber of images: 551
Filter: I+z
Binning: 1
Exposure time: 20.0 s
Output folder: /home/ferrais/SSOS/TS_8918_8919_B1R21_sp0900+2150

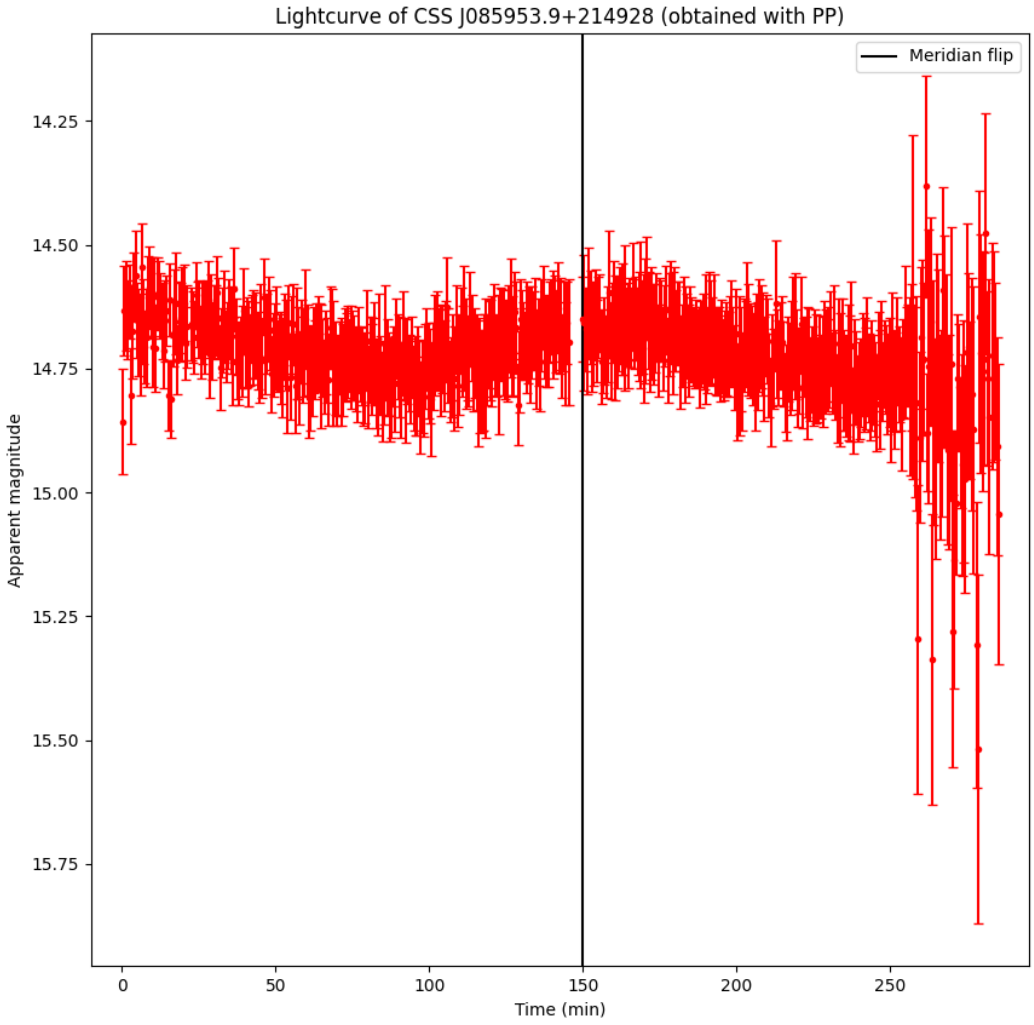

Appendix C

More lightcurves

We show 4 more lightcurves that we retrieved to demonstrate that we often have too few detection or data of insufficient quality in order to compute more rotation periods of asteroids.

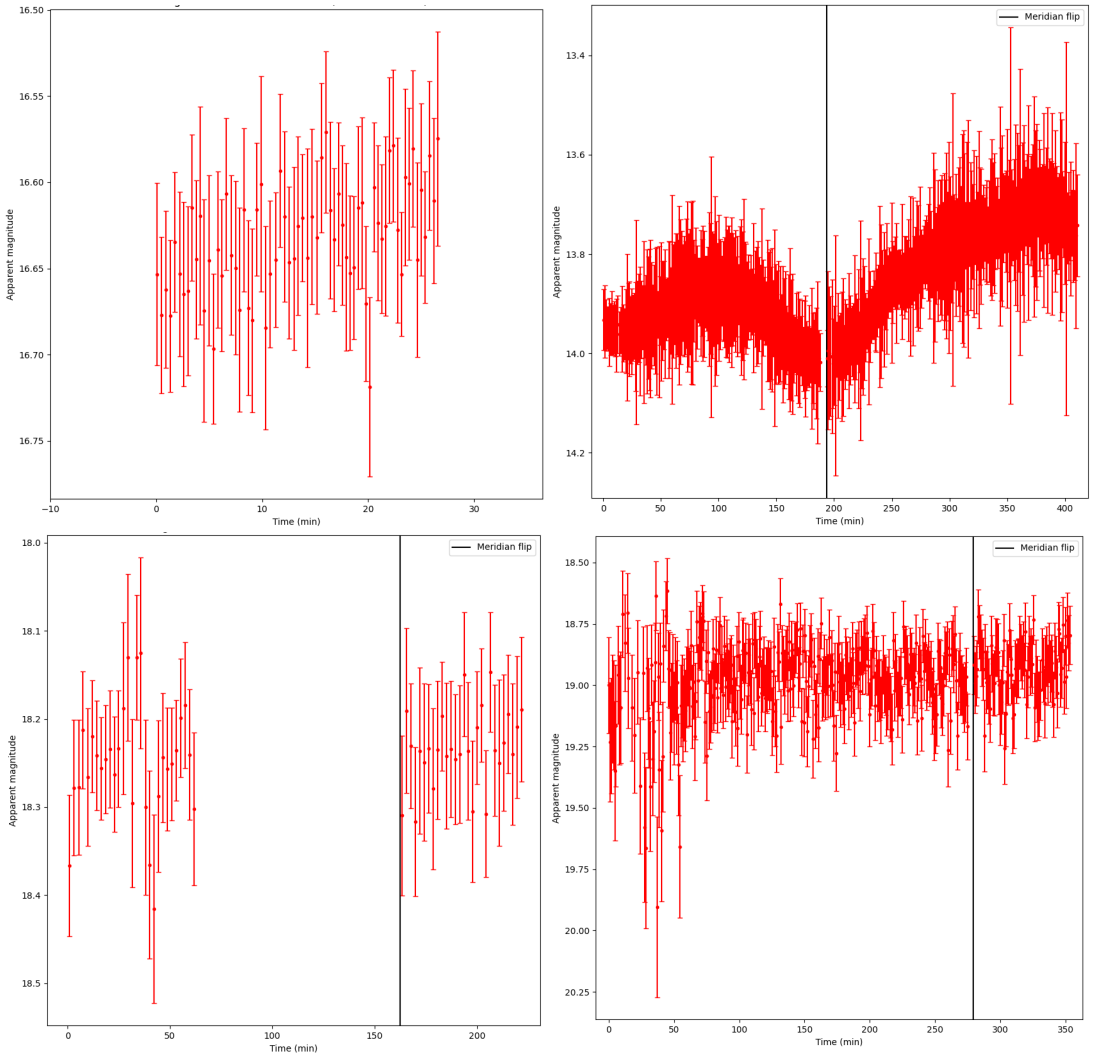

Figure C.1: From left to right and top to bottom: lightcurves of the asteroids 1991 DG, 1999 AP10, 2000 SZ121 and 2002 LP55.

Bibliography

[1] Guillaume Sicorello. Development of an automated pipeline to search for solar system objects in trappist data, 2020.

[2] Konstantin Batygin and Michael E. Brown. Evidence for a distant giant planet in the solar system. *The Astronomical Journal*, 151(2):22, Jan 2016.

[3] Michael E. Brown and Konstantin Batygin. Observational constraints on the orbit and location of planet nine in the outer solar system. *The Astrophysical Journal*, 824(2):L23, Jun 2016.

[4] Jakub Scholtz and James Unwin. What if planet 9 is a primordial black hole? *Physical Review Letters*, 125(5), Jul 2020.

[5] Kevin J. Walsh, Alessandro Morbidelli, Sean N. Raymond, David P. O'Brien, and Avi M. Mandell. A low mass for Mars from Jupiter's early gas-driven migration. *Nature*, 475(7355):206–209, July 2011.

[6] K. Tsiganis, R. Gomes, A. Morbidelli, and H. F. Levison. Origin of the orbital architecture of the giant planets of the Solar System. *Nature*, 435(7041):459–461, May 2005.

[7] A. Morbidelli, H. F. Levison, K. Tsiganis, and R. Gomes. Chaotic capture of Jupiter's Trojan asteroids in the early Solar System. *Nature*, 435(7041):462–465, May 2005.

[8] R. Gomes, H. F. Levison, K. Tsiganis, and A. Morbidelli. Origin of the cataclysmic Late Heavy Bombardment period of the terrestrial planets. *Nature*, 435(7041):466–469, May 2005.

[9] Kiyotsugu Hirayama. Groups of asteroids probably of common origin. *The Astrophysical Journal*, 31:185–188, October 1918.

[10] John J. Delgrande and Sidney V. Soanes. Kirkwood's Gap in the Asteroid Orbits. *Journal of the Royal Astronomical Society of Canada*, 37:187, June 1943.

[11] John M. C. Plane. Cosmic dust in the earth's atmosphere. *Chem. Soc. Rev.*, 41:6507–6518, 2012.

[12] Gareth S. Collins, H. Jay Melosh, and Robert A. Marcus. Earth impact effects program: A web-based computer program for calculating the regional environmental consequences of a meteoroid impact on earth. *Meteoritics & Planetary Science*, 40(6):817–840, 2005.

[13] D. J. Asher, M. Bailey, V. Emel'Yanenko, and W. Napier. Earth in the cosmic shooting gallery. *The Observatory*, 125:319–322, October 2005.

[14] Seth B. Nicholson. The Trojan Asteroids. *Leaflet of the Astronomical Society of the Pacific*, 8(381):239, January 1961.

[15] Martin Connors, Paul Wiegert, and Christian Veillet. Earth's Trojan asteroid. *Nature*, 475(7357):481–483, July 2011.

[16] C. de La Fuente Marcos and R. de La Fuente Marcos. Three new stable L5 Mars trojans. *Monthly Notices of the Royal Astronomical Society*, 432:L31–L35, May 2013.

[17] C. de la Fuente Marcos and R. de la Fuente Marcos. Asteroid 2014 YX_{49}: a large transient Trojan of Uranus. *Monthly Notices of the Royal Astronomical Society*, 467(2):1561–1568, May 2017.

[18] Apostolos A. Christou and Paul Wiegert. A population of Main Belt Asteroids co-orbiting with Ceres and Vesta. *Icarus*, 217(1):27–42, January 2012.

[19] J. Horner, N. W. Evans, and M. E. Bailey. Simulations of the population of Centaurs - I. The bulk statistics. *Monthly Notices of the Royal Astronomical Society*, 354(3):798–810, November 2004.

[20] F. Namouni and M. H. M. Morais. An interstellar origin for Jupiter's retrograde co-orbital asteroid. *Monthly Notices of the Royal Astronomical Society*, 477(1):L117–L121, June 2018.

[21] F Namouni and M H M Morais. An interstellar origin for high-inclination Centaurs. *Monthly Notices of the Royal Astronomical Society*, 494(2):2191–2199, 04 2020.

[22] Sarah Greenstreet, Brett Gladman, and Henry Ngo. Transient Jupiter Co-orbitals from Solar System Sources. *The Astronomical Journal*, 160(3):144, September 2020.

[23] A. Morbidelli, K. Batygin, R. Brasser, and S. N. Raymond. No evidence for interstellar planetesimals trapped in the Solar system. *Monthly Notices of the Royal Astronomical Society*, 497(1):L46–L49, September 2020.

[24] Aaron Do, Michael A. Tucker, and John Tonry. Interstellar interlopers: Number density and origin of 'oumuamua-like objects. *The Astrophysical Journal*, 855(1):L10, mar 2018.

[25] Karen Meech, Robert Weryk, Marco Micheli, Jan Kleyna, Olivier Hainaut, Robert Jedicke, Richard Wainscoat, Kenneth Chambers, Jacqueline Keane, Andreea Petric, Larry Denneau, Eugene Magnier, Travis Berger, Mark Huber, Heather Flewelling, C. Waters, Eva Schunova-Lilly, and Serge Chastel. A brief visit from a red and extremely elongated interstellar asteroid. *Nature*, 552:378–381, 12 2017.

[26] Zdenek Sekanina. 1i/'oumuamua as debris of dwarf interstellar comet that disintegrated before perihelion, 2019.

[27] David Jewitt and Jane Luu. Initial characterization of interstellar comet 2i/2019 q4 (borisov). *The Astrophysical Journal*, 886(2):L29, nov 2019.

[28] J. L. Elliot, S. D. Kern, K. B. Clancy, A. A. S. Gulbis, R. L. Millis, M. W. Buie, L. H. Wasserman, E. I. Chiang, A. B. Jordan, D. E. Trilling, and K. J. Meech. The Deep Ecliptic Survey: A Search for Kuiper Belt Objects and Centaurs. II. Dynamical Classification, the Kuiper Belt Plane, and the Core Population. *The Astronomical Journal*, 129(2):1117–1162, February 2005.

[29] J. H. Oort. The structure of the cloud of comets surrounding the Solar System and a hypothesis concerning its origin. *Bulletin of the Astronomical Institutes of the Netherlands*, 11:91–110, January 1950.

[30] Harold F. Levison and Luke Dones. Chapter 31 - comet populations and cometary dynamics. In Tilman Spohn, Doris Breuer, and Torrence V. Johnson, editors, *Encyclopedia of the Solar System (Third Edition)*, pages 705–719. Elsevier, Boston, third edition edition, 2014.

[31] E. Jehin, M. Gillon, D. Queloz, P. Magain, J. Manfroid, V. Chantry, M. Lendl, D. Hustemékers, and S. Udry. TRAPPIST: TRAnsiting PlanetesImals Small Telescope. *The Messenger*, 145:2–6, September 2011.

[32] Michaël Gillon, Amaury H. M. J. Triaud, Brice-Olivier Demory, Emmanuël Jehin, Eric Agol, Katherine M. Deck, Susan M. Lederer, Julien de Wit, Artem Burdanov, James G. Ingalls, Emeline Bolmont, Jeremy Leconte, Sean N. Raymond, Franck Selsis, Martin Turbet, Khalid Barkaoui, Adam Burgasser, Matthew R. Burleigh, Sean J. Carey, Aleksander Chaushev, Chris M. Copperwheat, Laetitia Delrez, Catarina S. Fernandes, Daniel L. Holdsworth, Enrico J. Kotze, Valérie Van Grootel, Yaseen Almleaky, Zouhair Benkhaldoun, Pierre Magain, and Didier Queloz. Seven temperate terrestrial planets around the nearby ultracool dwarf star TRAPPIST-1. *Nature*, 542(7642):456–460, February 2017.

[33] Marin Ferrais, Emmanuël Jehin, Jean Manfroid, Youssef Moulane, Francisco J. Pozuelos, Michaël Gillon, and Zouhair Benkhaldoun. Trappist Lightcurves of Main-Belt Asteroids 31 Euphrosyne, 41 Daphne and 89 Julia. *Minor Planet Bulletin*, 46(3):278–279, July 2019.

[34] E. Jehin, J. Manfroid, M. Gillon, D. Hutsemekers, and P. Magain. Occultation by (136199) Eris. *International Astronomical Union Circulars*, 9184:2, November 2010.

[35] E. Jehin, C. Opitom, J. Manfroid, D. Hutsemékers, and M. Gillon. The TRAPPIST comet survey. In K. Muinonen, A. Penttilä, M. Granvik, A. Virkki, G. Fedorets, O. Wilkman, and T. Kohout, editors, *Asteroids, Comets, Meteors 2014*, page 240, July 2014.

[36] M. Kaasalainen and J. Torppa. Optimization methods for asteroid lightcurve inversion: I. shape determination. *Icarus*, 153(1):24–36, 2001.

[37] M. Kaasalainen, S. Mottola, and M. Fulchignoni. *Asteroid Models from Disk-integrated Data*, pages 139–150. University of Arizona Press, 2002.

[38] M. Mahlke, E. Solano, H. Bouy, B. Carry, G.A. Verdoes Kleijn, and E. Bertin. The ssos pipeline: Identification of solar system objects in astronomical images. *Astronomy and Computing*, 28:100289, Jul 2019.

[39] Mahlke, M., Bouy, H., Altieri, B., Verdoes Kleijn, G., Carry, B., Bertin, E., de Jong, J. T. A., Kuijken, K., McFarland, J., and Valentijn, E. Mining the kilo-degree survey for solar system objects. *Astronomy & Astrophysics*, 610:A21, 2018.

[40] Bertin, E. and Arnouts, S. Sextractor: Software for source extraction. *Astronomy & Astrophysics Supplement Series*, 117(2):393–404, 1996.

[41] E. Bertin. Automatic Astrometric and Photometric Calibration with SCAMP. In C. Gabriel, C. Arviset, D. Ponz, and S. Enrique, editors, *Astronomical Data Analysis Software and Systems XV*, volume 351 of *Astronomical Society of the Pacific Conference Series*, page 112, July 2006.

[42] J. Berthier, F. Vachier, W. Thuillot, P. Fernique, F. Ochsenbein, F. Genova, V. Lainey, and J. E. Arlot. SkyBoT, a new VO service to identify Solar System objects. In C. Gabriel, C. Arviset, D. Ponz, and S. Enrique, editors, *Astronomical Data Analysis Software and Systems XV*, volume 351 of *Astronomical Society of the Pacific Conference Series*, page 367, July 2006.

[43] M. Mommert. Photometrypipeline: An automated pipeline for calibrated photometry. *Astronomy and Computing*, 18:47–53, 2017.

[44] A.W. Harris, J.W. Young, E. Bowell, L.J. Martin, R.L. Millis, M. Poutanen, F. Scaltriti, V. Zappalà, H.J. Schober, H. Debehogne, and K.W. Zeigler. Photoelectric observations of asteroids 3, 24, 60, 261, and 863. *Icarus*, 77(1):171–186, 1989.

[45] M. F. Skrutskie, R. M. Cutri, R. Stiening, M. D. Weinberg, S. Schneider, J. M. Carpenter, C. Beichman, R. Capps, T. Chester, J. Elias, J. Huchra, J. Liebert, C. Lonsdale, D. G. Monet, S. Price, P. Seitzer, T. Jarrett, J. D. Kirkpatrick, J. E. Gizis, E. Howard, T. Evans, J. Fowler, L. Fullmer, R. Hurt, R. Light, E. L. Kopan, K. A. Marsh, H. L. McCallon, R. Tam, S. Van Dyk, and S. Wheelock. The Two Micron All Sky Survey (2MASS). *The Astronomical Journal*, 131(2):1163–1183, February 2006.

[46] G. Pojmanski, B. Pilecki, and D. Szczygiel. The All Sky Automated Survey. Catalog of Variable Stars. V. Declinations 0 arcd - +28 arcd of the Northern Hemisphere. *Acta Astronomica*, 55:275–301, September 2005.

[47] T. Jayasinghe, K. Z. Stanek, C. S. Kochanek, B. J. Shappee, T. W. S. Holoien, Todd A. Thompson, J. L. Prieto, Subo Dong, M. Pawlak, O. Pejcha, J. V. Shields, G. Pojmanski, S. Otero, N. Hurst, C. A. Britt, and D. Will. The ASAS-SN catalogue of variable stars III: variables in the southern TESS continuous viewing zone. *Monthly Notices of the Royal Astronomical Society*, 485(1):961–971, May 2019.

[48] A. J. Drake, M. J. Graham, S. G. Djorgovski, M. Catelan, A. A. Mahabal, G. Torrealba, D. García-Álvarez, C. Donalek, J. L. Prieto, R. Williams, and et al. The catalina surveys periodic variable star catalog. *The Astrophysical Journal Supplement Series*, 213(1):9, Jun 2014.

[49] Daniel Huber, Stephen T. Bryson, Michael R. Haas, Thomas Barclay, Geert Barentsen, Steve B. Howell, Sanjib Sharma, Dennis Stello, and Susan E. Thompson. The k2 ecliptic plane input catalog (epic) and stellar classifications of 138,600 targets in campaigns 1–8. *The Astrophysical Journal Supplement Series*, 224(1):2, May 2016.

[50] Gaia Collaboration, T. Prusti, J. H. J. de Bruijne, A. G. A Brown, and Gaia team. The Gaia mission. *Astronomy & Astrophysics*, 595:A1, November 2016.

[51] Gaia Collaboration, Brown, A. G. A., Vallenari, A., Prusti, T., and Gaia team. Gaia early data release 3 - summary of the contents and survey properties. *Astronomy & Astrophysics*, 649:A1, 2021.

[52] N. N. Samus', E. V. Kazarovets, O. V. Durlevich, N. N. Kireeva, and E. N. Pastukhova. General catalogue of variable stars: Version GCVS 5.1. *Astronomy Reports*, 61(1):80–88, January 2017.

[53] K. C. Chambers, E. A. Magnier, N. Metcalfe, H. A. Flewelling, M. E. Huber, C. Z. Waters, L. Denneau, P. W. Draper, D. Farrow, D. P. Finkbeiner, C. Holmberg, J. Koppenhoefer, P. A. Price, A. Rest, R. P. Saglia, E. F. Schlafly, S. J. Smartt, W. Sweeney, R. J. Wainscoat, W. S. Burgett, S. Chastel, T. Grav, J. N. Heasley, K. W. Hodapp, R. Jedicke, N. Kaiser, R. P. Kudritzki, G. A. Luppino, R. H. Lupton, D. G. Monet, J. S. Morgan, P. M. Onaka, B. Shiao, C. W. Stubbs, J. L. Tonry, R. White, E. Bañados, E. F. Bell, R. Bender, E. J. Bernard, M. Boegner, F. Boffi, M. T. Botticella, A. Calamida, S. Casertano, W. P. Chen, X. Chen, S. Cole, N. Deacon, C. Frenk, A. Fitzsimmons, S. Gezari, V. Gibbs, C. Goessl, T. Goggia, R. Gourgue, B. Goldman, P. Grant, E. K. Grebel, N. C. Hambly, G. Hasinger, A. F. Heavens, T. M. Heckman, R. Henderson, T. Henning, M. Holman, U. Hopp, W. H. Ip, S. Isani, M. Jackson, C. D. Keyes, A. M. Koekemoer, R. Kotak, D. Le, D. Liska, K. S. Long, J. R. Lucey, M. Liu, N. F. Martin, G. Masci, B. McLean, E. Mindel, P. Misra, E. Morganson, D. N. A. Murphy, A. Obaika, G. Narayan, M. A. Nieto-Santisteban, P. Norberg, J. A. Peacock, E. A. Pier, M. Postman, N. Primak, C. Rae, A. Rai, A. Riess, A. Riffeser, H. W. Rix, S. Röser, R. Russel, L. Rutz, E. Schilbach, A. S. B. Schultz, D. Scolnic, L. Strolger, A. Szalay, S. Seitz, E. Small, K. W. Smith, D. R. Soderblom, P. Taylor, R. Thomson, A. N. Taylor, A. R. Thakar, J. Thiel, D. Thilker, D. Unger, Y. Urata, J. Valenti, J. Wagner, T. Walder, F. Walter, S. P. Watters, S. Werner, W. M. Wood-Vasey, and R. Wyse. The pan-starrs1 surveys, 2019.

[54] Xiaodian Chen. Wide-field Infrared Survey Explorer (WISE) Catalog of Periodic Variable Stars, July 2018.

[55] Xiaodian Chen, Shu Wang, Licai Deng, Richard de Grijs, Ming Yang, and Hao Tian. The Zwicky Transient Facility Catalog of Periodic Variable Stars, June 2020.